Physics – Uspekhi **60** (7) 643 – 666 (2017)

REVIEWS OF TOPICAL PROBLEMS PACS numbers: 12.39.Fe, 13.35.Dx, 13.66.Bc

Meson production processes in electron–positron collisions and tau-lepton decays within the extended Nambu – Jona-Lasinio model

M K Volkov, A B Arbuzov

DOI: https://doi.org/10.3367/UFNe.2016.11.037964

Contents

Abstract. The extended Nambu–Jona-Lasinio model is briefly described and various ways to apply it are demonstrated. Theoretical approaches to the low-energy meson production processes in colliding electron–positron beams and tau-lepton decays are reviewed. The processes considered occur via intermediate scalar, vector, and axial-vector mesons in the ground state and in the first radially excited state. The model uses the concept of spontaneous chiral symmetry breaking to describe such states. Experimental and theoretical comparisons with other phenomenological strong interaction models are presented.

Keywords: meson physics, chiral symmetry, electron–positron annihilation, tau lepton decays

M K Volkov Bogoliubov Laboratory of Theoretical Physics, Joint Institute for Nuclear Research, ul. Joliot-Curie 6, 141980 Dubna, Moscow region, Russian Federation
E-mail: volkov@theor.jinr.ru
A B Arbuzov Bogoliubov Laboratory of Theoretical Physics, Joint Institute for Nuclear Research, ul. Joliot-Curie 6, 141980 Dubna, Moscow region, Russian Federation; State University 'Dubna', ul. Universitetskaya 19, 141982 Dubna, Moscow region, Russian Federation
E-mail: arbuzov@theor.jinr.ru

Received 21 July 2016
Uspekhi Fizicheskikh Nauk **187** (7) 689 – 714 (2017)
DOI: https://doi.org/10.3367/UFNr.2016.11.037964
Translated by K A Postnov; edited by A M Semikhatov

1. Introduction

Electron–positron (e^-e^+) colliding beam experiments are an efficient way to study the properties of mesons and the nature of their interaction. Such colliders operate in many nuclear research centers worldwide, including VEPP-2000[1] (Budker Institute of Nuclear Physics of the Siberian Branch of the Russian Academy of Sciences, Novosibirsk), BEPC-II (Beijing Electron–Positron Collider II) (Beijing), Belle (High Energy Accelerator Research Organization (KEK), Japan), and BaBar (SLAC National Accelerator Laboratory, USA). These experiments actively study meson processes, including in the low-energy region below ~ 2 GeV of interest here. Equally interesting from this standpoint are the processes of pion production in τ-lepton decays. Remarkably, the pion production mechanisms in τ-lepton decays and in e^-e^+ annihilations are similar and can be described in a single approach.

To describe data obtained in colliding high-energy e^-e^+-beam experiments theoretically, the perturbation theory in quantum chromodynamics (QCD) can be used. But in the energy region of interest for us, the coupling constant of strong interactions is close to unity and the perturbation theory is inapplicable. Therefore, different phenomenological models are used there, which are typically based on the chiral symmetry of strong interactions [1] and the vector dominance theory for electromagnetic interactions [2]. A significant

[1] VEPP is the Russian abbreviation for colliding electron–positron beams.

shortcoming of most of these models is the need to introduce additional arbitrary constants to describe every new class of processes. As a result, the predictive power of such models is greatly reduced.

Among various phenomenological models of strong interactions, the Nambu–Jona-Lasinio (NJL) model is notable [3–12]. It is based on the QCD-motivated effective four-quark chiral symmetric interaction [13]. The model is implemented with a mechanism of spontaneous chiral symmetry breaking, enabling the masses of constituent quarks to be expressed in terms of masses of current quarks and the quark condensate. Remarkably, this model automatically includes vector dominance [6, 8, 14].

The NJL model successfully describes a range of physical properties of mesons, including the mass spectrum and their interactions at low energies, using a limited set of fixed parameters. In the NJL model framework, these parameters have a fundamental meaning: quark masses, the unique cutoff parameter of integrals in quark loops, two constants of the effective four-quark interaction, and the 't Hooft interaction parameter. To fix these parameters, the corresponding observables are used: the masses of π, K, η, and ρ mesons and the widths of decays $\pi^- \to \mu^-\nu_\mu$ and $\rho \to \pi\pi$. These parameters are kept fixed, which enables consecutive predictions of the mass spectrum of nonets of scalar, pseudoscalar, and vector mesons and of their low-energy interaction characteristics in good agreement with experimental data (see, e.g., reviews [8, 10, 12, 15, 16]).

The main goal of this review is to consider theoretical approaches to describing meson production processes in colliding e^-e^+ beams and in τ-lepton decays. At energies below 2 GeV, these processes, as noted above, have similar mechanisms: intermediate mesons play the leading role in both the ground and the first radially excited states. Indeed, higher radially excited states are too heavy and contribute little to the considered processes.

To take the excited states into account, the phenomenological models use different approaches, which assume the introduction of new degrees of freedom and additional parameters. In most models, the additional parameters are introduced for each new process separately. In this respect, of special interest is the extended Nambu–Jona-Lasinio model [11, 16–19], which enables taking the ground and radially excited states of mesons into account simultaneously. This model enables introducing the radially excited states using a polynomial form factor quadratic in the quark transverse momentum. The chiral symmetry and its spontaneous breaking mechanism are then preserved. The quark condensate value and masses of constituent quarks remain the same as in the standard NJL model. These requirements significantly restrict the number of additional model parameters.

The structure of this review is as follows. In Section 2, we describe the extended Nambu–Jona-Lasinio (ENJL) model for nonets of pseudoscalar and vector mesons and for isovector charged scalar kaons. In Section 3, the Primakoff processes and photoproduction of pions and η mesons in collider e^-e^+ beam experiments are considered. In Section 4, we present the results for different meson production processes in e^-e^+ annihilation. Section 5 describes semilepton decays of τ leptons. In Sections 3–5, we systematically compare the results obtained in the framework of other phenomenological models. In Section 6, the general analysis of the obtained results is presented.

2. Extended Nambu–Jona-Lasinio model

The chiral-symmetric four-quark interaction with local currents has the form

$$\mathcal{L}_{\rm int}^{(4)} = \frac{G_1}{2}\int \mathrm{d}^4x \sum_{j=1}^{9}\sum_{i=1}^{2}\left[J^j_{S,i}(x)J^j_{S,i}(x) + J^j_{P,i}(x)J^j_{P,i}(x)\right] - \int \mathrm{d}^4x \sum_{j=1}^{9}\sum_{i=1}^{2}\left(\frac{G_2}{2}\,J^{j,\mu}_{V,i}(x)J^j_{V,i,\mu}(x) + \frac{G_3}{2}\,J^{j,\mu}_{A,i}(x)J^j_{A,i,\mu}(x)\right), \tag{1}$$

where G_i are the coupling constants. The scalar (S), pseudoscalar (P), vector (V), and axial-vector (A) quark currents are

$$J^j_{S(P),i}(x) = \int \mathrm{d}^4x_1\,\mathrm{d}^4x_2\;\bar q(x_1)F^j_{S(P),i}(x;x_1,x_2)q(x_2)\,, \qquad J^{j,\mu}_{V(A),i}(x) = \int \mathrm{d}^4x_1\,\mathrm{d}^4x_2\;\bar q(x_1)F^{j,\mu}_{V(A),i}(x;x_1,x_2)q(x_2)\,, \tag{2}$$

where $\bar q = (\bar u, \bar d, \bar s)$ are the u, d, and s quark fields. The values of the main model parameters and means of their determination in terms of the observed quantities are described in [18, 20]. To describe mesons containing quarks, the 't Hooft interaction [21, 22] is also introduced. The form factors $F(x;x_1,x_2)$ for the local interaction describing the ground states of mesons are expressed as

$$F^j_{S,1}(x;x_1,x_2) = \tau^j\delta(x_1-x)\delta(x_2-x)\,, \quad F^j_{P,1}(x;x_1,x_2) = \mathrm{i}\gamma_5\tau^j\delta(x_1-x)\delta(x_2-x)\,, \quad F^{j,\mu}_{V,1}(x;x_1,x_2) = \gamma^\mu\tau^j\delta(x_1-x)\delta(x_2-x)\,, \quad F^{j,\mu}_{A,1}(x;x_1,x_2) = \gamma_5\gamma^\mu\tau^j\delta(x_1-x)\delta(x_2-x)\,, \tag{3}$$

where γ^μ and γ_5 are the standard Dirac matrices.

To describe the excited states, nonlocal form factors are used, which have quite a complicated form in the coordinate representation (see [17]). Below, we work in the momentum representation, in which the form factors have a simpler form:

$$F^j_{S,2}(\mathbf{k}^2) = \tau^j c^j_S f_j(\mathbf{k}^2)\,, \quad F^j_{P,2}(\mathbf{k}^2) = \mathrm{i}\gamma_5\tau^j c^j_P f_j(\mathbf{k}^2)\,, \quad F^{j,\mu}_{V,2}(\mathbf{k}^2) = \gamma^\mu\tau^j c^j_V f_j(\mathbf{k}^2)\,, \quad F^{j,\mu}_{A,2}(\mathbf{k}^2) = \gamma_5\gamma^\mu\tau^j c^j_A f_j(\mathbf{k}^2)\,, \tag{4}$$

where c^j_S, c^j_P, c^j_V, and c^j_A are coefficients in the form factors of the excited states of mesons. The index $j = 1,\ldots,9$ defines the basis elements τ^j of the flavor group U(3) [23]. This basis is slightly different from the standard Gell-Mann matrices λ:

$$\tau_k = \lambda_k\,, \quad k = 1,\ldots,7\,, \qquad \tau_8 = \frac{\lambda_0+\lambda_8}{\sqrt{3}} = \begin{pmatrix}1&0&0\\0&1&0\\0&0&0\end{pmatrix}, \qquad \tau_9 = \frac{-\lambda_0+\sqrt{2}\lambda_8}{\sqrt{3}} = \begin{pmatrix}0&0&0\\0&0&0\\0&0&-\sqrt{2}\end{pmatrix}. \tag{5}$$

To describe the first radially excited states, we introduce the functions $f_j(\mathbf{k}^2)$ in the form of a quadratic polynomial in the three-dimensional quark momentum,[2]

$$f_j(\mathbf{k}^2) \equiv 1 + d_j\mathbf{k}^2 \,. \tag{6}$$

The slope parameters d_j are uniquely determined from the requirement that taking the excited states into account does not change the quark condensate value, which is equivalent to the condition that the constituent quark masses are constant. This requirement reduces to the vanishing of the one-loop integral with one quark propagator (a 'tadpole' type) with one form factor at the vertex:

$$-\mathrm{i}N_\mathrm{c}\,\mathrm{tr}\int_{\Lambda_3}\frac{\mathrm{d}^4k}{2\pi^4}\,\frac{f_j(\mathbf{k}^2)}{\hat{k}-m} = 0\,, \tag{7}$$

where the constituent quark mass m is either $m_\mathrm{u} = m_\mathrm{d} = 280$ MeV or $m_\mathrm{s} = 420$ MeV; $\Lambda_3 = 1.03$ GeV is the three-dimensional momentum cutoff parameter [18, 20]; and $N_\mathrm{c} = 3$ is the number of quark colors. The slope parameter is somewhat different for light (u and d) and strange (s) quarks: $d_\mathrm{u} = -1.784\ \mathrm{GeV}^{-2}$ and $d_\mathrm{s} = -1.727\ \mathrm{GeV}^{-2}$. It is important to note that these values are not arbitrary model parameters; this is not so with the coefficients c_U^j, however, which are determined by the masses of excited meson states. We note that the functions $f_j(\mathbf{k}^2)$ determine the interaction between mesons.

We also include the six-quark 't Hooft interaction [21, 22], which has the form

$$\mathcal{L}_\mathrm{int}^{(6)} = -K\Big\{\det\big[\bar{q}(1+\gamma_5)q\big] + \det\big[\bar{q}(1-\gamma_5)q\big]\Big\}\,, \tag{8}$$

where K is the 't Hooft interaction constant. To include this interaction in the original Lagrangian of the NJL model (1), one contraction of quark fields (by all possible means) is required, which gives rise to the appearance of a nondiagonal interaction between light and strange quarks. This allows solving the $\mathrm{U_A}(1)$ problem and describing the states of isoscalar η and η' mesons [10, 15, 22].

With the 't Hooft interaction, the four-quark NJL Lagrangian can be represented in the form [16, 24]

$$\begin{aligned}
\mathcal{L}(\bar{q},q) &= \int \mathrm{d}^4x\,\bar{q}(x)(\mathrm{i}\partial\!\!\!/ - m^0)q(x)\\
&+\frac{1}{2}\int \mathrm{d}^4x\sum_{a=1}^{9}\sum_{b=1}^{9}\big[G_{ab}^{(-)}J_{S,1}^a(x)J_{S,1}^b(x) + G_{ab}^{(+)}J_{P,1}^a(x)J_{P,1}^b(x)\big]\\
&+\int \mathrm{d}^4x\sum_{a=1}^{9}\frac{G_a}{2}\big[J_{S,2}^a(x)J_{S,2}^a(x) + J_{P,2}^a(x)J_{P,2}^a(x)\big]\\
&-\frac{G_2}{2}\int \mathrm{d}^4x\sum_{a=1}^{9}\sum_{i=1}^{2}J_{V,i}^{a,\mu}(x)J_{V,i,\mu}^a(x)\\
&-\frac{G_3}{2}\int \mathrm{d}^4x\sum_{a=1}^{9}\sum_{i=1}^{2}J_{A,i}^{a,\mu}(x)J_{A,i,\mu}^a(x)\,,
\end{aligned} \tag{9}$$

where m^0 is the current quark mass,

$$\begin{aligned}
&G_{11}^{\pm} = G_{22}^{\pm} = G_{33}^{\pm} = G_1 \pm 4Km_\mathrm{s}I_1(m_\mathrm{s})\,,\\
&G_{44}^{\pm} = G_{55}^{\pm} = G_{66}^{\pm} = G_{77}^{\pm} = G_1 \pm 4Km_\mathrm{u}I_1(m_\mathrm{u})\,,\\
&G_{88}^{\pm} = G_1 \mp 4Km_\mathrm{s}I_1(m_\mathrm{s})\,,\quad G_{99}^{\pm} = G_1\,,\\
&G_{89}^{\pm} = G_{98}^{\pm} = \pm 4\sqrt{2}Km_\mathrm{u}I_1(m_\mathrm{u})\,,\\
&G_{ab} = 0\,,\quad a\neq b,\quad a,b = 1,\ldots,7.
\end{aligned} \tag{10}$$

We introduce the general notation for loop integrals that appear in calculations:

$$\begin{aligned}
I_n^{(l)}(m) &= -\mathrm{i}N_\mathrm{c}\int\frac{\mathrm{d}^4k}{(2\pi)^4}\,\frac{f^l(\mathbf{k}^2)}{(k^2-m^2+\mathrm{i}0)^n}\\
&\times\Theta(\Lambda_3^2-\mathbf{k}^2)\,,\qquad l = 0,1,2\,.
\end{aligned} \tag{11}$$

Here, Θ is the Heaviside theta-function. The constant before the excited states of scalar and pseudoscalar mesons is

$$G_a = G_1(c_P^a)^2\,. \tag{12}$$

After standard bosonization, we obtain

$$\begin{aligned}
&L_(\bar{q},q;\sigma,\varphi,V,A) = \int \mathrm{d}^4x_1\int \mathrm{d}^4x_2\,\bar{q}(x_1)\\
&\times\Bigg[(\mathrm{i}\partial\!\!\!/_{x_2} - m^0)\delta(x_1-x_2)\\
&+\int \mathrm{d}^4x\sum_{i=1}^{2}\sum_{a=1}^{9}\Big(\sigma_i^a(x)F_{\sigma,i}^a(x;x_1,x_2) + \varphi_i^a(x)F_{\varphi,i}^a(x;x_1,x_2)\\
&+V_{i,\mu}^a(x)F_{V,i}^{a,\mu}(x;x_1,x_2) + A_{i,\mu}^a(x)F_{A,i}^{a,\mu}(x;x_1,x_2)\Big)\Bigg]q(x_2)\\
&-\sum_{a,b=1}^{9}\int \mathrm{d}^4x\Bigg\{\frac{1}{2}\Big[\big(G_{ab}^-\big)^{-1}\sigma_1^a(x)\sigma_1^b(x)\\
&+\big(G_{ab}^+\big)^{-1}\varphi_1^a(x)\varphi_1^b(x)\Big] - \frac{1}{2G_V}\Big[\big(V_1^{a,\mu}(x)\big)^2 + \big(A_1^{a,\mu}(x)\big)^2\Big]\Bigg\}\\
&-\int \mathrm{d}^4x\Bigg\{\frac{1}{2G_1}\Big[\big(\sigma_2^a(x)\big)^2 + \big(\phi_2^a(x)\big)^2\Big]\\
&-\frac{1}{2G_V}\Big[\big(V_2^{a,\mu}(x)\big)^2 + \big(A_2^{a,\mu}(x)\big)^2\Big]\Bigg\}\,.
\end{aligned} \tag{13}$$

Here, φ, V, and A are pseudoscalar, vector, and axial-vector fields.

Among the boson fields introduced, scalar isoscalar fields $\sigma_1^{8,9}$ with nonzero vacuum expectation values $\langle\sigma_1^{8,9}\rangle = \sigma_0^{8,9} \neq 0$ are of special interest. By an identity transformation (subtracting vacuum expectations from $\sigma_1^{8,9}$ and adding them to the current quark masses m^0), we pass to physical fields and obtain the constituent quark masses instead of current masses [10, 17]:

$$m_\mathrm{u}^0 = m_\mathrm{u}\big(1 - 8G_{88}^{(-)}I_1^{(0)}(m_\mathrm{u})\big)\,, \tag{14}$$

$$m_\mathrm{s}^0 = m_\mathrm{s}\big(1 - 8G_{99}^{(-)}I_1^{(0)}(m_\mathrm{s})\big)\,. \tag{15}$$

In this review, we restrict ourselves to describing electron–positron annihilation into hadrons and τ-lepton decays with a minimal number of mesons (no more than three) in the final state.

2.1 Lagrangian for pions

Formula (13) for the free Lagrangian of pion fields in the one-loop approximation after renormalization of meson fields

[2] The form factors in fact depend on the transverse part of the quark momentum $k^\perp \equiv k - (kP/P^2)P$, where P is the 4-momentum of a meson. In the meson rest frame, the transverse momentum takes the simple form $\mathbf{k}^\perp = \{0,\mathbf{k}\}$. Therefore, we take $\mathbf{k}$ as the argument.

yields (see [18, 25] for the details)

$$L^{(2)}(\pi_{1,2}) = -\pi_1^2\,\frac{M_{\pi_1}^2}{2} - \pi_2^2\,\frac{M_{\pi_2}^2}{2} + \frac{P^2}{2}(\pi_1^2 + 2R_\pi\pi_1\pi_2 + \pi_2^2)\,. \tag{16}$$

Here, P is the meson momentum operator,

$$R_\pi = \frac{I_2^{(1)}(m_u)\sqrt{Z}}{\sqrt{I_2^{(0)}(m_u)I_2^{(2)}(m_u)}}\,, \tag{17}$$

where we have taken the $\pi - a_1$ transitions into account, and

$$Z = 1 - \frac{6m_u^2}{M_{a_1}^2}\,. \tag{18}$$

We note that two renormalizations of meson fields have been made. The first is due to the reduction in the kinetic terms to the normal form by absorbing the integrals I_2 arising from quark loops into the meson fields. The second renormalization is due to taking the possible transitions between pions and axial-vector mesons into account. This gives rise to the appearance of the additional dipole factor $\sqrt{Z}$ before the renormalization coefficient for the pion ground states [8]. A similar renormalization for the excited states can be disregarded because the corresponding coefficient is $\sqrt{\bar{Z}} = (1 - R_\pi^2 6m_u^2/M_{a_1}^2)^{1/2} \approx 1$ (see [18]).

The unphysical meson masses are determined as

$$\begin{aligned} M_{\pi_1}^2 &= g_{\pi_1}^2\left(\frac{1}{G_\pi} - 8I_1^{(0)}(m_u)\right),\\ M_{\pi_2}^2 &= g_{\pi_2}^2\left(\frac{1}{(c^\pi)^2 G_1} - 8I_1^{(2)}(m_u)\right), \end{aligned} \tag{19}$$

where $G_\pi = G_{11}^+$ and $c^\pi = c_P^1$. The constants $g_{\pi_1} = (4ZI_2^{(0)}(m_u))^{-1/2}$ and $g_{\pi_2} = (4I_2^{(2)}(m_u))^{-1/2}$ are the pion field renormalization constants. After renormalizations, they also turn into the quark–meson coupling constants in Lagrangian (13).

The diagonalization of Lagrangian (16) yields the standard free Lagrangian for physical fields:

$$L^{(2)}(\pi,\pi') = -\pi^2\,\frac{M_\pi^2}{2} - \pi'^2\,\frac{M_{\pi'}^2}{2} + \frac{P^2}{2}\left(\pi^2 + \pi'^2\right). \tag{20}$$

Here, the masses of π and $\pi' \equiv \pi(1300)$ mesons are expressed in terms of the masses of unphysical mesons M_{π_1,π_2} as [18, 19, 25]

$$\begin{aligned} M_\pi^2(M_{\pi'}^2) = \frac{1}{2(1-R_\pi^2)}\Big[&M_{\pi_1}^2 + M_{\pi_2}^2\\ &- (+)\sqrt{(M_{\pi_1}^2 - M_{\pi_2}^2)^2 + (2M_{\pi_1}M_{\pi_2}R_\pi)^2}\,\Big]. \end{aligned} \tag{21}$$

This diagonalization is performed by the transformation

$$\begin{aligned} \pi_1 &= \frac{\sin(\alpha+\alpha_0)\pi - \cos(\alpha+\alpha_0)\pi'}{\sqrt{Z}\sin(2\alpha_0)}\,,\\ \pi_2 &= \frac{\sin(\alpha-\alpha_0)\pi - \cos(\alpha-\alpha_0)\pi'}{\sin(2\alpha_0)}\,. \end{aligned} \tag{22}$$

We note that these transformations of pion fields are nonunitary, because, in addition to rotation, they include a rescaling related to the renormalization. The mixing angles can be found from the expressions

$$\begin{aligned} \sin\alpha_0 &= \sqrt{\frac{1+R_\pi}{2}},\\ \tan(2\alpha-\pi) &= \sqrt{\frac{1}{R_\pi^2} - 1}\,\frac{M_{\pi_1}^2 - M_{\pi_2}^2}{M_{\pi_1}^2 + M_{\pi_2}^2}\,. \end{aligned} \tag{23}$$

As a result, the quark–pion interaction takes the form

$$\begin{aligned} L(\pi,q) = \bar{q}(p')\Big\{&A_\pi\gamma_5\left[\tau^3\pi^0(k) + \sqrt{2}\,\tau^+\pi^+(k)\right.\\ &\left. + \sqrt{2}\,\tau^-\pi^-(k)\right] - A_{\pi'}\gamma_5\left[\tau^3(\pi^0)'(k)\right.\\ &\left. + \sqrt{2}\,\tau^+(\pi^+)'(k) + \sqrt{2}\,\tau^-(\pi^-)'(k)\right]\Big\}q(p) \end{aligned} \tag{24}$$

with $k = p' - p$, where p' and p are quark momenta, $\tau^\pm = (\tau^1 \pm i\tau^2)/\sqrt{2}$, and

$$\begin{aligned} A_\pi &= g_{\pi_1}\,\frac{\sin(\alpha+\alpha_0)}{\sin(2\alpha_0)} + g_{\pi_2}f_u(\mathbf{k}^2)\,\frac{\sin(\alpha-\alpha_0)}{\sin(2\alpha_0)}\,,\\ A_{\pi'} &= g_{\pi_1}\,\frac{\cos(\alpha+\alpha_0)}{\sin(2\alpha_0)} + g_{\pi_2}f_u(\mathbf{k}^2)\,\frac{\cos(\alpha-\alpha_0)}{\sin(2\alpha_0)}\,, \end{aligned}$$

where $f_u(\mathbf{k}^2)$ is the form factor for light quarks defined by formula (6).

The parameters G_1 and c^π can be determined from the values of masses M_{π_1} and M_{π_2} in Eqns (19), which are in turn expressed in terms of masses of physical pions:

$$\begin{aligned} M_{\pi_1}^2(M_{\pi_2}^2) &= \gamma\,\frac{M_\pi^2 + M_{\pi'}^2}{2}\\ &\quad - (+)\sqrt{\gamma^2\,\frac{(M_\pi^2 + M_{\pi'}^2)^2}{4} - \gamma M_\pi^2 M_{\pi'}^2}\,,\\ \gamma &= 1 - R_\pi^2\,. \end{aligned} \tag{25}$$

However, there is also a third, so far nonfixed, parameter, the 't Hooft coupling constant K. This parameter is deduced from the η and η' masses in Section 2.5 [see formula (42)].

2.2 Lagrangian for vector mesons

In a similar way, the ENJL model can be constructed for vector mesons ρ, ω, and ϕ. After the renormalization $V^\mu \to V_r^\mu$, the free Lagrangian of the model for unphysical vector mesons takes the form

$$\begin{aligned} L^{(2)}(\rho,\omega,\phi) &= -\frac{1}{2}\sum_{i,j=1}^{2}\sum_{a=1}^{5} V_{r,i}^{\mu,a}R_{i,j}^{\mu\nu}V_{r,j}^{\nu,a}\,,\\ R_{11}^{\mu\nu} &= g^{\mu\nu}P^2 - P^\mu P^\nu - g^{\mu\nu}M^2(V_1^a)\,,\\ R_{22}^{\mu\nu} &= g^{\mu\nu}P^2 - P^\mu P^\nu - g^{\mu\nu}M^2(V_2^a)\,,\\ R_{12}^{\mu\nu} &= R_{21}^{\mu\nu} = R_{V^a}\left(g^{\mu\nu}P^2 - P^\mu P^\nu\right),\\ R_{V^b}\Big|_{b=1,2,3,4} &\equiv R_{V_u} = \frac{I_2^{(1)}(m_u)}{\sqrt{I_2^{(0)}(m_u)I_2^{(2)}(m_u)}}\,, \end{aligned}$$

$$
\begin{aligned}
&R_{V^5} \equiv R_{V_s} = \frac{I_2^{(1)}(m_s)}{\sqrt{I_2^{(0)}(m_s) I_2^{(2)}(m_s)}}\,,\\
&M^2(V_1^b) = M^2(\rho_1, \omega_1) = \frac{g_{\rho_1}^2}{4G_2}\,,\\
&M^2(V_2^b) = M^2(\rho_2, \omega_2) = \frac{g_{\rho_2}^2}{4G_2 (c^\rho)^2}\,,\\
&g_\rho^2 \equiv g_{\rho_1}^2 = \frac{3}{2I_2^{(0)}(m_u)}\,, \qquad g_{\rho_2}^2 = \frac{3}{2I_2^{(2)}(m_u)}\,,\\
&M^2(V_1^5) = M^2(\phi_1) = \frac{g_{\phi_1}^2}{4G_2}\,,\\
&M^2(V_2^5) = M^2(\phi_2) = \frac{g_{\phi_2}^2}{4G_2 (c^\phi)^2}\,,\\
&g_{\phi_1}^2 = \frac{3}{2I_2^{(0)}(m_s)}\,, \qquad g_{\phi_2}^2 = \frac{3}{2I_2^{(2)}(m_s)}\,.
\end{aligned}
\tag{26}
$$

The free Lagrangian for vector mesons is diagonalized using angles β_0^u, β^u, β_0^s, and β^s:

$$
\begin{aligned}
&\sin\beta_0^{u,s} = \sqrt{\frac{1 + R_{V^{b,5}}}{2}}\,,\\
&\tan(2\beta^{u,s} - \pi) = \sqrt{\frac{1}{R_{V^{b,5}}^2} - 1}\,\frac{M^2(V_1^{b,5}) - M^2(V_2^{b,5})}{M^2(V_1^{b,5}) + M^2(V_2^{b,5})}\,.
\end{aligned}
\tag{27}
$$

After transformations analogous to those made for pion fields, we obtain the Lagrangian for interactions of physical vector mesons with quarks:

$$
\begin{aligned}
&L(\rho, \omega, \phi; q) = \bar q(p') \Bigg[\sum_{a=1}^{3} A_\rho \tau_a \hat\rho_a(k) + A_\omega \tau_8 \hat\omega(k) + A_\phi \tau_9 \hat\phi(k)\\
&\quad - \sum_{a=1}^{3} A_{\rho'} \tau_a \hat\rho_a'(k) - A_{\omega'} \tau_8 \hat\omega'(k) - A_{\phi'} \tau_9 \hat\phi'(k) \Bigg] q(p)\,,\\
&k = p' - p, \qquad \rho^\pm = \frac{\rho_1 \pm i\rho_2}{\sqrt{2}}, \qquad \hat V \equiv V^\mu \gamma_\mu\,,\\
&A_\rho = A_\omega = \frac{g_{\rho_1}}{2}\,\frac{\sin(\beta^u + \beta_0^u)}{\sin(2\beta_0^u)} + \frac{g_{\rho_2}}{2} f(\mathbf{k}^2)\,\frac{\sin(\beta^u - \beta_0^u)}{\sin(2\beta_0^u)}\,,\\
&A_{\rho'} = A_{\omega'} = \frac{g_{\rho_1}}{2}\,\frac{\cos(\beta^u + \beta_0^u)}{\sin(2\beta_0^u)} + \frac{g_{\rho_2}}{2} f(\mathbf{k}^2)\,\frac{\cos(\beta^u - \beta_0^u)}{\sin(2\beta_0^u)}\,,\\
&A_\phi = \frac{g_{\phi_1}}{2}\,\frac{\sin(\beta^s + \beta_0^s)}{\sin(2\beta_0^s)} + \frac{g_{\phi_2}}{2} f(\mathbf{k}^2)\,\frac{\sin(\beta^s - \beta_0^s)}{\sin(2\beta_0^s)}\,,\\
&A_{\phi'} = \frac{g_{\phi_1}}{2}\,\frac{\cos(\beta^s + \beta_0^s)}{\sin(2\beta_0^s)} + \frac{g_{\phi_2}}{2} f(\mathbf{k}^2)\,\frac{\cos(\beta^s - \beta_0^s)}{\sin(2\beta_0^s)}\,.
\end{aligned}
$$

2.3 Lagrangian for K mesons

In the ENJL model, the Lagrangian for the interaction of strange mesons with quarks has the form

$$
\begin{aligned}
&\Delta L_{\text{int}}(q, \bar q, K, K_0^*, K^*) = \bar q \Bigg[i\gamma^5 \sum_{j=+,-} \tau_j \big(a_K K^j + b_K \tilde K^j\big)\\
&\quad + \sum_{j=+,-} \tau_j \big(a_{K_0^*} K_0^{*j} + b_{K_0^*} \tilde K_0^{*j}\big)\\
&\quad + \frac{1}{2}\gamma^\mu \sum_{j=+,-} \tau_j \big(a_{K^*} K_\mu^{*j} + b_{K^*} \tilde K_\mu^{*j}\big) \Bigg] q\,,
\end{aligned}
\tag{28}
$$

where $K^\pm$, $K_0^{*\pm}$, and $K^{*\pm}$ are the respective pseudoscalar, scalar, and vector-strange mesons. Their first radially excited states are marked by a tilde over the symbols; τ_+ and τ_- are the matrices

$$
\begin{aligned}
&\tau_+ = \frac{\lambda_4 + i\lambda_5}{\sqrt{2}} = \sqrt{2}\begin{pmatrix} 0 & 0 & 1\\ 0 & 0 & 0\\ 0 & 0 & 0 \end{pmatrix},\\
&\tau_- = \frac{\lambda_4 - i\lambda_5}{\sqrt{2}} = \sqrt{2}\begin{pmatrix} 0 & 0 & 0\\ 0 & 0 & 0\\ 1 & 0 & 0 \end{pmatrix}.
\end{aligned}
\tag{29}
$$

The coefficients a_r and b_r resulting from the diagonalization of the original Lagrangian for kaons are

$$
\begin{aligned}
&a_r = \frac{1}{\sin(2\theta_r^0)} \Big[g_r \sin(\theta_r + \theta_r^0) + g_r' f_{us}(\mathbf{k}^2) \sin(\theta_r - \theta_r^0) \Big],\\
&b_r = -\frac{1}{\sin(2\theta_r^0)} \Big[g_r \cos(\theta_r + \theta_r^0) + g_r' f_{us}(\mathbf{k}^2) \cos(\theta_r - \theta_r^0) \Big],\\
&r = K,\ K_0^*,\ K^*\,.
\end{aligned}
\tag{30}
$$

2.4 Lagrangian for η mesons

After bosonizing, taking two-vertex quark loops with different η mesons at the ends into account, and renormalizing similarly to the pion case, we arrive at a nondiagonal free Lagrangian for isoscalar fields:

$$
L^{(2)}(\Phi) = \frac{1}{2} \sum_{i,j=1}^{4} \Phi_i \mathcal{K}_{ij}(P) \Phi_j\,,
\tag{31}
$$

where $\Phi = (\varphi_1^8, \varphi_2^8, \varphi_1^9, \varphi_2^9)$,

$$
\begin{aligned}
&\mathcal{K}_{11}(P) = P^2 - M_{\varphi_1^8}^2\,,\\
&\mathcal{K}_{22}(P) = P^2 - M_{\varphi_2^8}^2\,,\\
&\mathcal{K}_{33}(P) = P^2 - M_{\varphi_1^9}^2\,,\\
&\mathcal{K}_{44}(P) = P^2 - M_{\varphi_2^9}^2\,,\\
&\mathcal{K}_{12}(P) = \mathcal{K}_{21}(P) = R_{\eta_u} P^2\,,\\
&\mathcal{K}_{34}(P) = \mathcal{K}_{43}(P) = R_{\eta_s} P^2\,,\\
&\mathcal{K}_{13}(P) = \mathcal{K}_{31}(P) = g_{s_1} g_{s_2}\,\frac{2}{G_{89}^+}\,,\\
&\mathcal{K}_{14}(P) = \mathcal{K}_{41}(P) = \mathcal{K}_{24}(P) = \mathcal{K}_{42}(P) = 0\,,\\
&\mathcal{K}_{23}(P) = \mathcal{K}_{32}(P) = 0\,,\\
&R_{\eta_u} = R_\pi\,, \qquad R_{\eta_s} = R_{V^5}\,,\\
&g_{s_1} = \frac{1}{\sqrt{4I_2^{(0)}(m_s)}}\,, \qquad g_{s_2} = \frac{1}{\sqrt{4I_2^{(2)}(m_s)}}\,.
\end{aligned}
\tag{32}
$$

The masses of unphysical mesons are

$$
\begin{aligned}
&M_{\varphi_1^8}^2 = g_{\pi_1}^2 \left(\frac{1}{G_{88}^-} - 8I_1(m_u) \right),\\
&M_{\varphi_2^8}^2 = g_{\pi_2}^2 \left(\frac{1}{(c_P^8)^2 G_1} - 8I_1^{(2)}(m_u) \right),\\
&M_{\varphi_1^9}^2 = g_{s_1}^2 \left(\frac{1}{G_{99}^-} - 8I_1(m_s) \right),\\
&M_{\varphi_2^9}^2 = g_{s_2}^2 \left(\frac{1}{(c_P^9)^2 G_1} - 8I_1^{(2)}(m_s) \right).
\end{aligned}
\tag{33}
$$

Table 1. Mixing matrix coefficients for η mesons.

$R_{i,j}$	η	$\hat{\eta}$	η'	$\hat{\eta}'$
φ_1^8	0.71	0.62	−0.32	0.56
φ_2^8	0.11	−0.87	−0.48	−0.54
φ_1^9	0.62	0.19	0.56	−0.67
φ_2^9	0.06	−0.66	0.30	0.82

The transition to physical fields $\Phi_{\rm ph} = (\eta, \hat{\eta}, \eta', \hat{\eta}')$ is made by numerically diagonalizing the matrix $\mathcal{K}_{ij}$. As a result, the mixing matrix [25] is obtained, which is presented in Table 1. This matrix allows describing the interaction of physical η mesons with quarks in terms of the previously defined interactions of unphysical mesons:

$$L_{\rm int}(\eta, q) = \bar{q}(k')\left(\mathrm{i}\gamma_5 \sum_{j=8,9} \tau_j \sum_{\boldsymbol{\eta}=\eta,\eta',\hat{\eta},\hat{\eta}'} A^j_{\boldsymbol{\eta}}\boldsymbol{\eta}(p)\right) q(k)\,,$$
$$A^j_{\eta,\hat{\eta},\eta',\hat{\eta}'} = g_{j,1} b^{\varphi^j_1}_{\eta,\hat{\eta},\eta',\hat{\eta}'} + g_{j,2} b^{\varphi^j_2}_{\eta,\hat{\eta},\eta',\hat{\eta}'} f_j(\mathbf{k}^2)\,, \tag{34}$$

where $g_{8,1} = g_{\pi_1}$, $g_{8,2} = g_{\pi_2}$, $g_{9,1} = g_{s_1}$, $g_{9,2} = g_{s_2}$, and the coefficients $b^{\varphi^j_2}_{\eta,\hat{\eta},\eta',\hat{\eta}'}$ are elements of the mixing matrix presented in Table 1.

2.5 Values of model parameters

In the NJL model, the Goldberger–Treiman relation holds, which follows from the calculation of the $\pi^\pm \to \mu^\pm \nu_\mu$ decay width:

$$g_{\pi_1} \equiv g_\pi = \frac{m_{\rm u}}{F_\pi}\,, \tag{35}$$

where F_π is the pion decay constant. On the other hand [8],

$$\frac{m_{\rm u}^2}{F_\pi^2} = Z^{-1}\,\frac{g_\rho^2}{6} = \left(1 - \frac{6m_{\rm u}^2}{m_{a_1}^2}\right)^{-1}\frac{g_\rho^2}{6}\,. \tag{36}$$

From (36), using experimental values of the parameters $F_\pi \approx 92.8$ MeV, $g_\rho \approx 6.14$, and $m_{a_1} \approx 1230$ MeV, we find $m_{\rm u} = 280$ MeV. The strange quark mass $m_{\rm s} = 420$ MeV was fixed in [26] in terms of the experimental values of K-meson masses. The calculated mass of the φ meson in the model was in satisfactory agreement with experimental results.

The parameter g_ρ is expressed in terms of the integral $I_2^{(0)}$ depending on the cutoff parameter Λ_3 [see Eqns (26)]. This implies that $\Lambda_3 = 1.03$ GeV. The values of the cutoff parameter, the quark masses, and the slope parameters of the form factors can be used to calculate the integrals though which the coupling constants of quark–meson interactions are expressed:

$$g_{\rho_2} = 9.87\,, \quad g_{\pi_2} = \frac{g_{\rho_2}}{\sqrt{6}} = 4.03\,,$$
$$g_{s_1} = 3.00\,, \quad g_{s_2} = 5.28\,, \tag{37}$$
$$g_{\phi_1} = 7.34\,, \quad g_{\phi_2} = 12.54\,.$$

We also obtain

$$R_{V_{\rm u}} \approx 0.545\,, \quad R_{\eta_{\rm u}} = R_\pi = \sqrt{Z}\,R_{V_{\rm u}} \approx 0.474\,,$$
$$R_{\eta_{\rm s}} = R_{V_{\rm s}} \approx 0.411\,, \quad Z \approx 0.69\,. \tag{38}$$

The mixing angles of the excited and nonexcited pions $\alpha_0 \approx 59.12^\circ$ and $\alpha \approx 59.48^\circ$ were obtained in [18, 19]. The corresponding angles for the φ mesons are $\beta_0^{\rm s} \approx 57.13^\circ$ and $\beta^{\rm s} \approx 68.4^\circ$. For the ρ mesons, $\beta_0 \approx 61.5^\circ$ and $\beta \approx 81.8^\circ$.

For completeness, we present some values of integrals with two propagators and different numbers of form factors:

$$I_2^{(0)}(m_{\rm u}) \approx 0.0398\,, \quad I_2^{(1)}(m_{\rm u}) \approx 0.0135\,,$$
$$I_2^{(2)}(m_{\rm u}) \approx 0.0154\,. \tag{39}$$

The from-factor slope parameters and the mixing angles for kaons have the values

$$d_{\rm us} = -1.761\ \mathrm{GeV}^{-2}\,,$$
$$\theta_{\rm K} = 58.11^\circ\,, \quad \theta_{\rm K_0^*} = 74^\circ\,, \quad \theta_{\rm K^*} = 84.74^\circ\,, \tag{40}$$
$$\theta^0_{\rm K} = 55.52^\circ\,, \quad \theta^0_{\rm K_0^*} = 60^\circ\,, \quad \theta^0_{\rm K^*} = 59.56^\circ\,.$$

The coupling constants are

$$g_{\rm K} = \left(\frac{4}{Z_{\rm K}}\,I_2^{(0)}(m_{\rm u}, m_{\rm s})\right)^{-1/2} \approx 3.77\,,$$
$$g'_{\rm K} = \left(4I_2^{(0)}(m_{\rm u}, m_{\rm s})\right)^{-1/2} \approx 4.69\,,$$
$$g_{\rm K_0^*} = \left(4I_2^{(0)}(m_{\rm u}, m_{\rm s})\right)^{-1/2} \approx 2.78\,,$$
$$g'_{\rm K_0^*} = \left(4I_2^{(0)}(m_{\rm u}, m_{\rm s})\right)^{-1/2} \approx 4.69\,,$$
$$g_{\rm K^*} = \left(\frac{2}{3}\,I_2^{(0)}(m_{\rm u}, m_{\rm s})\right)^{-1/2} \approx 6.81\,,$$
$$g'_{\rm K^*} = \left(\frac{2}{3}\,I_2^{(n)}(m_{\rm u}, m_{\rm s})\right)^{-1/2} \approx 11.49\,,$$
$$I_2^{(n)}(m_1, m_2) = -\mathrm{i}\,\frac{N_{\rm c}}{(2\pi)^4}\int \mathrm{d}^4k\,\Theta(\Lambda_3^2 - \mathbf{k}^2)\,\frac{f^n_{1,2}(\mathbf{k}^2)}{(m_1^2 - k^2)(m_2^2 - k^2)}\,,$$
$$Z_{\rm K} = \left[1 - \frac{3}{2}\,\frac{(m_{\rm u} + m_{\rm s})^2}{M^2_{\rm K_1}}\right]^{-1} \approx 1.83\,. \tag{41}$$

The diagonalization yields the masses of the ground and first radially excited states of the corresponding mesons, which are presented in Table 2 in comparison with experimental values [27] (we take the masses of neutral mesons).

In diagonalizing the free Lagrangian of the η mesons, the following model parameters have been used:

$$G_1 = 3.14\ \mathrm{GeV}^{-2}\,, \quad K = 6.1\ \mathrm{GeV}^{-5}\,,$$
$$c_P^8 = 1.50\,, \quad c_P^9 = 1.66, \quad c^\pi = 144\,. \tag{42}$$

Table 2. Masses of pseudoscalar and vector mesons.

Meson	$M^{\rm theor}$, MeV	$M^{\rm exp}$, MeV
π	136	134.9766(6)
π(1300)	1300	1300(100)
K	490	497.611(13)
K(1460)	1300	∼ 1460
ρ	768	775.26(25)
ρ(1450)	1490	1465 (25)
K*(892)	887	891.66(26)
K*(1410)	1479	1414(15)
$\mathrm{K}_0^*(800)$	900	682(29)
$\mathrm{K}_0^*(1430)$	1500	1425(50)
φ(1020)	1019	1019.461(19)
φ(1680)	1682	1680(20)

Here, we show the value of the parameter c^{π} entering the pion mass definition (19).

The diagonalization of the free Lagrangian results in finding the masses of physical η mesons:

$$M_{\eta} = 520\ \text{MeV}\,, \quad M_{\eta'} = 910\ \text{MeV}\,, \\ M_{\hat{\eta}} = 1280\ \text{MeV}\,, \quad M_{\hat{\eta}'} = 1470\ \text{MeV}\,. \tag{43}$$

The corresponding experimental values are

$$M_{\eta}^{\text{exp}} \approx 548\ \text{MeV}\,, \quad M_{\eta'}^{\text{exp}} \approx 958\ \text{MeV}\,, \\ M_{\hat{\eta}}^{\text{exp}} = M_{\eta(1295)} \approx 1294\ \text{MeV}\,, \\ M_{\hat{\eta}'}^{\text{exp}} = M_{\eta(1475)} \approx 1476\ \text{MeV}\,. \tag{44}$$

When considering the η mesons, we have taken only quark–antiquark states into account and ignored their possible mixing with the pseudoscalar glueball.

3. Radiative decays and meson photoproduction processes

This section is devoted to describing two-photon decays of neutral pseudoscalar mesons in both the ground and the first radially excited states. We also consider the leading two-particle radiative decays of pseudoscalar and vector mesons in the ground and the first radially excited states. In addition, we present the results for different cross-symmetric processes with the production of neutral pseudoscalar mesons, which are studied in electron–positron colliders.

3.1 Two-photon decays of pions and η mesons

The two-photon decay of a neutral pion, which is the principal decay mode, has been studied both experimentally and theoretically by many authors. When studying this process, we encounter the problem known as the Adler–Bell–Jackiw anomaly (see [28] for a detailed discussion). In the standard NJL model, this process is described in review [8], as are similar decays of the η and η′ mesons.

In the ENJL model, the decay cross section of the ground and excited states of pions into two photons has the form [29]

$$\Gamma_{\pi\to\gamma\gamma} = \left(\frac{\alpha}{\pi}\right)^2 \frac{M_{\pi}^3}{16\pi m_{\text{u}}^2} \left[I_0^{(3)}(m_{\text{u}}) g_{\pi_1} \frac{\sin(\alpha+\alpha_0)}{\sin(2\alpha_0)} \right. \\ \left. + I_1^{(3)}(m_{\text{u}}) g_{\pi_2} \frac{\sin(\alpha-\alpha_0)}{\sin(2\alpha_0)} \right]^2 = 8.0\ \text{eV}\,, \tag{45}$$

$$\Gamma_{\pi'\to\gamma\gamma} = \left(\frac{\alpha}{\pi}\right)^2 \frac{M_{\pi'}^3}{16\pi m_{\text{u}}^2} \left[I_0^{(3)}(m_{\text{u}}) g_{\pi_1} \frac{\cos(\alpha+\alpha_0)}{\sin(2\alpha_0)} \right. \\ \left. + I_1^{(3)}(m_{\text{u}}) g_{\pi_2} \frac{\cos(\alpha-\alpha_0)}{\sin(2\alpha_0)} \right]^2 = 1.0\ \text{eV}\,. \tag{46}$$

The modern experimental value of the $\pi^0 \to \gamma\gamma$ decay width is (7.7 ± 0.2) eV. The $\pi(1300) \to \gamma\gamma$ decay width obtained in the model is the theoretical prediction to be tested experimentally. When calculating the integral $I_0^{(3)}(m_{\text{u}})$, we are dealing with an anomalous triangle diagram that represents the Wess–Zumino term. The integral converges, and therefore no cutoff is used. However, if a cutoff is used, the chiral symmetry of the Wess–Zumino sector of the chiral Lagrangian is broken.

Table 3. Theoretical (Γ^{theor}) and experimental (Γ^{exp}) values of the decay width Γ of η mesons into two photons.

Meson / Γ, eV	η(550)	η(1295)	η(958)	η(1475)
Γ^{theor}	520	93	4990	230
Γ^{exp}	510 ± 26	—	4340 ± 140	—

Two-photon decays of the η mesons can be described similarly [30]. For example, the η(550) two-photon decay amplitude is

$$T_{\eta\to\gamma\gamma} = \frac{\alpha}{9\pi}\, \varepsilon_{\mu\nu\rho\sigma} q_1^{\rho} q_2^{\sigma} \epsilon_1^{\mu} \epsilon_2^{\nu} \\ \times \left(R_{1,1} \frac{g_{\pi}}{m_{\text{u}}} 5I_3^{(0)}(m_{\text{u}}) + R_{2,1} \frac{g_{\pi_2}}{m_{\text{u}}} 5I_3^{(1)}(m_{\text{u}}) \right. \\ \left. - R_{3,1} \frac{g_{\text{s}_1}}{m_{\text{s}}} \sqrt{2}\, I_3^{(0)}(m_{\text{s}}) - R_{4,1} \frac{g_{\text{s}_2}}{m_{\text{s}}} \sqrt{2}\, I_3^{(1)}(m_{\text{s}}) \right), \tag{47}$$

where $\varepsilon_{\mu\nu\rho\sigma}$ is the Levi-Civita tensor, $q_{1,2}^{\rho,\sigma}$ and $\epsilon_{1,2}^{\mu,\nu}$ are the momenta and polarization vectors of photons, and $R_{i,j}$ are the elements of the mixing matrix of the η mesons (see Table 1). Numerical values of the two-photon decay widths of four states of the η mesons are listed in Table 3.

3.2 Radiative decays of vector and pseudoscalar mesons

Radiative decays of pseudoscalar and vector mesons with one photon in the final state, which are described by the anomalous triangle quark diagrams (Fig. 1), are very similar to the two-photon decays of pseudoscalar mesons considered above. Such radiative decays for the ground state of light pseudoscalar and vector mesons π, η, η′, ρ, ω, and ϕ are well studied experimentally. Studies of the corresponding decays with the participation of radially excited states of these mesons are carried out on modern accelerators, including VEPP-2000 and BEPC-II. The ENJL model predicts the decay widths of these processes. Corresponding results were obtained in [31] (Table 4). Table 4 shows that the ENJL model does not cardinally change the standard NJL model results for the ground states of mesons, which are in good agreement with the experimental data. This allows us to hope that predictions of this model for processes with radially excited states are reasonable.

3.3 Photoproduction of neutral pseudoscalar mesons by leptons

We now turn to the processes of meson production in electron–positron accelerators.

We start by considering the generation of pseudoscalar mesons in e^-e^+ beams through intermediate photons:

$$e^-(p_1) + e^+(p_2) \to e^-(p_1') + e^+(p_2') + P(p)\,, \tag{48}$$

where $P = \pi$, $\pi(1300)$, η, η′, $\eta(1295)$, and $\eta(1475)$. In the leading approximation, the total cross section of the two-

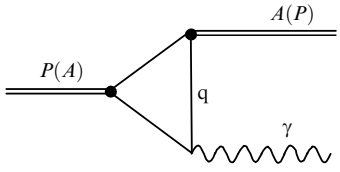

Figure 1. Amplitude of radiative decays of pseudoscalar (P) and vector (A) mesons with a quark triangle loop $q = (u, d, s)$.

Table 4. Widths of one-photon radiative decays in the standard and extended NJL models in comparison with experimental data [27].

Γ, keV / Decay	NJL	ENJL	PDG*
$\rho \to \eta\gamma$	52.1	45.5	44.7
$\omega \to \eta\gamma$	6.2	5.5	3.9
$\phi \to \eta\gamma$	30.9	32.01	55.3
$\phi \to \eta'\gamma$	0.267	0.257	0.27
$\eta' \to \rho\gamma$	49.9	69.4	57.7
$\eta' \to \omega\gamma$	5.03	6.9	5.5
$\eta(1295) \to \rho\gamma$	—	12.6	—
$\eta(1295) \to \omega\gamma$	—	1.4	—
$\eta(1295) \to \phi\gamma$	—	7.6	—
$\eta(1475) \to \rho\gamma$	—	11.9	—
$\eta(1475) \to \omega\gamma$	—	2.9	—
$\eta(1475) \to \phi\gamma$	—	8.1	—
$\rho \to \pi\gamma$	89.8	81.7	89.4
$\omega \to \pi\gamma$	832	756	703
$\pi(1300) \to \rho\gamma$	—	26.2	—
$\pi(1300) \to \omega\gamma$	—	229	—

* Particle Data Group Collaboration.

photon production process has the form [32]

$$\sigma_P = (4\alpha)^2 \ln^2\left(\frac{\sqrt{s}}{2m_e}\right) \frac{\Gamma_{P\to\gamma\gamma}}{M_P^3}\, Y\left(\frac{M_P^2}{s}\right), \qquad Y(z) = (2+z)^2 \ln\frac{1}{\sqrt{z}} - (3+z)(1-z). \tag{49}$$

Numerical results [30] and the corresponding experimental data [33] for η mesons with the total center-of-mass energy of colliding beams $\sqrt{s} = 29$ GeV are presented in Table 5. For pions [29] with the total energy of the beams $\sqrt{s} = 3$ GeV, the predicted values are $\sigma_\pi \approx 0.43$ nb and $\sigma_{\pi(1300)} \approx 0.09$ nb.

We now consider the Primakoff processes with pion and η-meson production on a charged lepton [29]:

$$\gamma(k) + l(p) \to P(p_1) + l(p'), \quad l = e, \mu, \qquad p^2 = p'^2 = m_l^2, \quad k^2 = 0, \quad p_1^2 = M_P^2, \qquad s = 2kp > M_P^2 \gg m_l^2. \tag{50}$$

The cross section is dominated by kinematics with the exchange of an almost real photon with the momentum $q = p - p'$. In this case, calculations are conveniently performed using the Sudakov parameterization:

$$q = a\tilde{p} + bk + q_\perp, \quad q^2 = -\frac{\mathbf{q}^2 + a^2 m_l^2}{1-a}, \qquad a = \frac{\mathbf{q}^2 + M_P^2}{s}. \tag{51}$$

The differential cross section has the form

$$d\sigma^{\gamma l\to Pl} = \frac{\alpha\Gamma(P\to\gamma\gamma)}{M_P^3}\left[1 + \left(1 - \frac{M_P^2}{s}\right)^2\right] \frac{\mathbf{q}^2\, d\mathbf{q}^2}{(\mathbf{q}^2 + m_l^2\, M_P^4/s^2)^2}. \tag{52}$$

Table 5. Total two-photon production cross sections σ of pseudoscalar mesons.

Meson / σ, nb	$\eta(550)$	$\eta(1295)$	$\eta(958)$	$\eta(1475)$
σ^{theor}	1.4	0.014	2.1	0.022
σ^{exp}	1.25 ± 0.13	—	1.8 ± 0.3	—

The total cross section of the process is

$$\sigma^{\gamma l\to Pl} = \frac{\alpha\Gamma(P\to\gamma\gamma)}{M_P^3}\left[1 + \left(1 - \frac{M_P^2}{s}\right)^2\right]\left(\ln\frac{s^2}{m_l^2 M_P^2} - 1\right). \tag{53}$$

For the energy $\sqrt{s} = 3$ GeV, we obtain the total cross sections $\sigma^{\gamma e\to\pi e} = 0.37$ nb, $\sigma^{\gamma e\to\pi' e} = 0.14$ nb, $\sigma^{\gamma e\to\eta e} = 0.33$ nb, $\sigma^{\gamma e\to\eta' e} = 0.54$ nb, $\sigma^{\gamma e\to\eta(1295)e} = 3.6$ pb, and $\sigma^{\gamma e\to\eta(1475)e} = 5.7$ pb.

4. Meson production in electron–positron annihilations

In this section, we consider production of light mesons in e^-e^+ annihilations at the center-of-mass energies up to 2 GeV. These processes occur with the participation of intermediate mesons in both ground and radially excited states. Experimental data show that the ground and first radially excited states of intermediate vector mesons make the greatest contribution to these processes. We note that the ENJL model can quite satisfactorily describe exactly these states. In Sections 4.1–4.5, we describe the following processes: $e^+ + e^- \to P + \gamma$, where $P = \pi$, $\pi(1300)$, η, η', $\eta(1295)$, and $\eta(1475)$; $e^+ + e^- \to \pi + \omega$; $e^+ + e^- \to \pi^+ + \pi^-$; and $e^+ + e^- \to \eta 2\pi$.

4.1 Processes $e^+ + e^- \to P + \gamma$

The amplitude of the process $e^+ + e^- \to \pi^0 + \gamma$ is determined by four contributions (Figs 2–4):

$$T^\lambda = \bar{e}\gamma_\mu e\varepsilon_{\mu\lambda\alpha\beta}\frac{p_\pi^\alpha p_\gamma^\beta}{s m_u}\left(B_\gamma + B_{\rho+\omega} + B_\phi + B_{\rho'+\omega'}\right), \tag{54}$$

where $s = (p_1(e^+) + p_2(e^-))^2$. We ignore the contribution from the intermediate $\phi(1680)$, because its $\pi\gamma$ decay has a low probability.

The contribution from the contact diagram with photon exchange (see Fig. 2) is

$$B_\gamma = 2V_{\gamma^*\pi^0\gamma}, \quad V_{\gamma^*\pi^0\gamma} = g_{\pi_1} I_3^{(0)}. \tag{55}$$

The nonexcited intermediate ρ and ω mesons give

$$B_{\rho+\omega} = \left[\frac{\sin(\beta+\beta_0)}{\sin(2\beta_0)} + R_{V_u}\frac{\sin(\beta-\beta_0)}{\sin(2\beta_0)}\right] \times \left(\frac{s}{s - M_\rho^2 + iM_\rho\Gamma_\rho} + \frac{s}{s - M_\omega^2 + iM_\omega\Gamma_\omega}\right)\frac{V_{\rho\pi^0\gamma}}{g_{\rho_1}}, \qquad V_{\rho\pi^0\gamma} = g_{\pi_1}\left[\frac{\sin(\beta+\beta_0) g_{\rho_1} I_3^{(0)}}{\sin(2\beta_0)} + \frac{\sin(\beta-\beta_0) g_{\rho_2} I_3^{(1)}}{\sin(2\beta_0)}\right]. \tag{56}$$

The first factor in the expression for $B_{\rho+\omega}$ takes the splitting of the vector vertex in the $\gamma - \rho(\omega)$ transition into account. This splitting appears in the extended model to describe the mixing

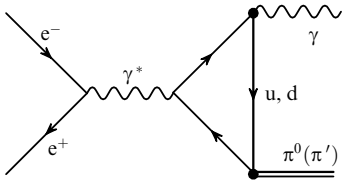

Figure 2. Feynman diagram of the $e^+e^- \to \pi^0\gamma$ process with an intermediate photon.

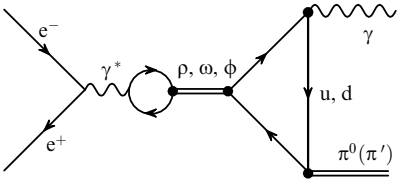

Figure 3. Feynman diagram of the $e^+e^- \to \pi^0\gamma$ process with intermediate ρ, ω, and ϕ mesons.

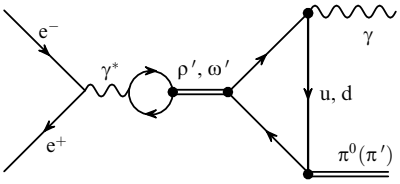

Figure 4. Feynman diagram of the $e^+e^- \to \pi^0\gamma$ process with intermediate excited ρ' and ω'.

the ρ_1 and ρ_2 states in the physical ρ meson. The general structure of the $\gamma-\rho(\omega,\phi)$ transition via a quark loop is described in [8].

The transition of the intermediate ϕ meson into $\pi^0\gamma$ occurs due to its mixing with the ω meson:

$$B_\phi = \frac{\sqrt{2}}{3}\,\frac{s\sin\theta_{\omega\phi}}{s-M_\phi^2+\mathrm{i}M_\phi\Gamma_\phi}\,\frac{V_{\omega\pi^0\gamma}}{g_{\rho_1}}\,,$$
$$V_{\omega\pi^0\gamma} = 3V_{\rho\pi^0\gamma}\,. \tag{57}$$

The mixing angle is $\theta_{\omega\phi}\approx -3^\circ$ [12, 15, 34].

The contribution of the intermediate ρ' and ω' mesons has the form

$$B_{\rho'+\omega'} = \left[-\frac{\cos(\beta+\beta_0)}{\sin(2\beta_0)} - R_{V_u}\frac{\cos(\beta-\beta_0)}{\sin(2\beta_0)}\right]\frac{1}{g_{\rho_1}} \times\left(\frac{s}{s-M_{\rho'}^2+\mathrm{i}M_{\rho'}\Gamma_{\rho'}}+\frac{s}{s-M_{\omega'}^2+\mathrm{i}M_{\omega'}\Gamma_{\omega'}}\right)V_{\rho'\pi^0\gamma}\,,$$
$$V_{\rho'\pi^0\gamma} = -g_{\pi_1}\left[\frac{\cos(\beta+\beta_0)g_{\rho_1}I_3^{(0)}}{\sin(2\beta_0)}+\frac{\cos(\beta-\beta_0)g_{\rho_2}I_3^{(1)}}{\sin(2\beta_0)}\right]. \tag{58}$$

The process cross section is

$$\sigma^{e^+e^-\to\pi\gamma}(s) = \frac{\alpha^3}{24\pi^2 s^3 f_\pi^2}\,\lambda^{3/2}(s,M_\omega^2,M_\pi^2)\,\frac{1}{g_{\pi_1}^2} \times\left|B_\gamma + B_{\rho+\omega} + B_\phi + B_{\rho'+\omega'}\right|^2,$$
$$\lambda(s,M_\omega^2,M_\pi^2) = (s-M_\omega^2-M_\pi^2)^2 - 4M_\omega^2M_\pi^2\,. \tag{59}$$

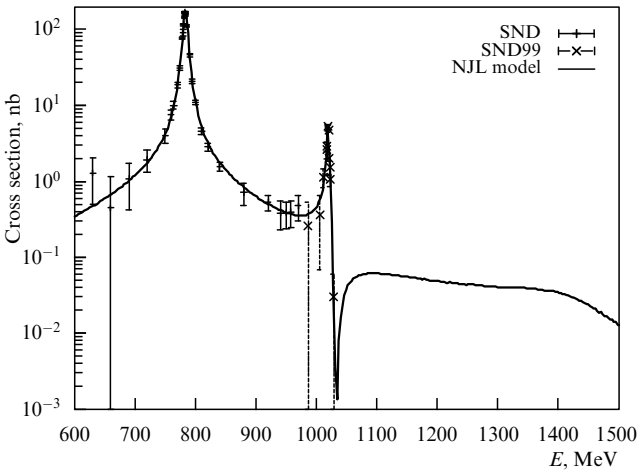

Figure 5. Cross section of the process $e^+e^- \to \pi^0\gamma$ as a function of energy.

A comparison of the calculated cross section of this process in the ENJL model with experimental data [35–37] is presented in Fig. 5. These calculations used the masses and widths of mesons in [27], with the exception of the width $\Gamma_{\rho'}$, which was assumed to be 340 MeV, one standard deviation below the central experimental value. Our results are also in agreement with the generalized vector dominance model calculations [38].

The $e^+ + e^- \to \pi'(1300) + \gamma$ process is described similarly; the main difference is in the modification of the vertices $V_{\gamma^*(\rho,\rho',\omega,\omega')\pi'\gamma}$:

$$V_{\gamma^*\pi'\gamma} = V_{\gamma^*\pi^0\gamma}\frac{\cos(\alpha+\alpha_0)}{\sin(2\alpha_0)} + g_{\pi_2}I_1^{(3)}\,\frac{\cos(\alpha-\alpha_0)}{\sin(2\alpha_0)}\,,$$
$$V_{\rho\pi'\gamma} = -g_{\rho_1}\frac{\sin(\beta+\beta_0)}{\sin(2\beta_0)}\,g_{\pi_1}\,\frac{\cos(\alpha+\alpha_0)}{\sin(2\alpha_0)}\,I_0^{(3)} - g_{\rho_2}\frac{\sin(\beta-\beta_0)}{\sin(2\beta_0)}\,g_{\pi_1}\,\frac{\cos(\alpha+\alpha_0)}{\sin(2\alpha_0)}\,I_1^{(3)} - g_{\rho_1}\frac{\sin(\beta+\beta_0)}{\sin(2\beta_0)}\,g_{\pi_2}\,\frac{\cos(\alpha-\alpha_0)}{\sin(2\alpha_0)}\,I_1^{(3)} - g_{\rho_2}\frac{\sin(\beta-\beta_0)}{\sin(2\beta_0)}\,g_{\pi_2}\,\frac{\cos(\alpha-\alpha_0)}{\sin(2\alpha_0)}\,I_2^{(3)}\,,$$
$$V_{\rho'\pi'\gamma} = g_{\rho_1}\frac{\cos(\beta+\beta_0)}{\sin(2\beta_0)}\,g_{\pi_1}\,\frac{\cos(\alpha+\alpha_0)}{\sin(2\alpha_0)}\,I_0^{(3)} + g_{\rho_2}\frac{\cos(\beta-\beta_0)}{\sin(2\beta_0)}\,g_{\pi_1}\,\frac{\cos(\alpha+\alpha_0)}{\sin(2\alpha_0)}\,I_1^{(3)} + g_{\rho_1}\frac{\cos(\beta+\beta_0)}{\sin(2\beta_0)}\,g_{\pi_2}\,\frac{\cos(\alpha-\alpha_0)}{\sin(2\alpha_0)}\,I_1^{(3)} + g_{\rho_2}\frac{\cos(\beta-\beta_0)}{\sin(2\beta_0)}\,g_{\pi_2}\,\frac{\cos(\alpha-\alpha_0)}{\sin(2\alpha_0)}\,I_2^{(3)}\,. \tag{60}$$

All other factors are exactly the same as in $\pi^0\gamma$ production. The predicted cross section of the $\pi(1300)\gamma$ production is shown in Fig. 6.

4.2 Processes $e^+e^- \to [\eta, \eta', \eta(1295), \eta(1475)]\gamma$

Electron–positron annihilation into the $\eta\gamma$ pair was studied experimentally in the VEPP-2M collider [39]. Similar processes producing η' mesons and the first radially excited

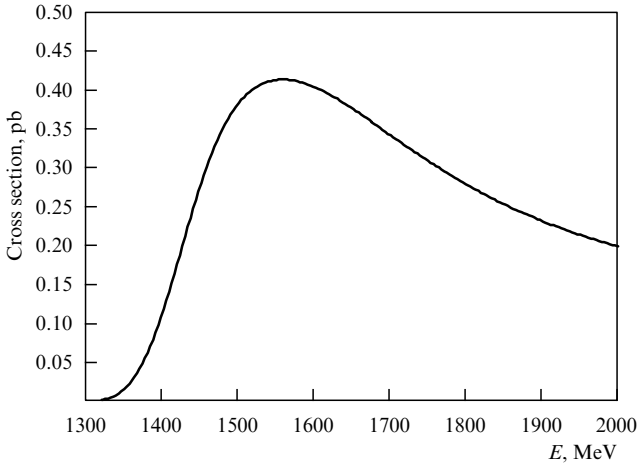

Figure 6. Cross section of the process $e^+e^- \to \pi^0(1300)\gamma$ as a function of energy in the NJL model.

η mesons will be studied using the modified VEPP-2000 collider. In the ENJL model, this process is described in [40].

The structure of the amplitude of processes with $\eta_i\gamma$ pair production is very similar to that presented in Section 4.1 for the $\pi\gamma$ pair production. Here, we include the contributions from the intermediate photon and ρ, ω, and ϕ mesons both in the ground and first radially excited states. Especially important are the contributions from the intermediate ϕ and ϕ' mesons, because the η mesons contain both ud-quark and s-quark structures. The amplitude has the form

$$T^\lambda = \bar{e}\gamma^\mu e\,\frac{p_\eta^\alpha p_\gamma^\beta}{s}\,\{T_\gamma + T_{\rho+\omega} + T_\phi + T_{\rho'+\omega'} + T_{\phi'}\}\varepsilon_{\mu\lambda\alpha\beta}\,, \tag{61}$$

where contributions from the intermediate states are

$$\begin{aligned}
T_\gamma &= \frac{2}{3}\left(5\,\frac{16}{3}\,\pi^2 m_u V_{\gamma u} + \sqrt{2}\,\frac{16}{3}\,\pi^2 m_s V_{\gamma s}\right),\\
T_{\rho+\omega} &= \left(\frac{3s}{m_\rho^2 - s - i\sqrt{s}\,\Gamma_\rho} + \frac{1}{3}\,\frac{s}{m_\omega^2 - s - i\sqrt{s}\,\Gamma_\omega}\right)\\
&\quad\times\frac{C_{\gamma\rho}}{g_{\rho_1}}\left(\frac{16}{3}\,\pi^2 m_u V_\rho\right),\\
T_\phi &= -\frac{2\sqrt{2}}{3}\,\frac{s}{m_\phi^2 - s - i\sqrt{s}\,\Gamma_\phi}\,\frac{C_{\gamma\phi}}{g_{\phi_1}}\left(\frac{16}{3}\,\pi^2 m_s V_\phi\right),\\
T_{\rho'+\omega'} &= \left(\frac{3s}{m_{\rho'}^2 - s - i\sqrt{s}\,\Gamma_{\rho'}(s)} + \frac{1}{3}\,\frac{s}{m_{\omega'}^2 - s - i\sqrt{s}\,\Gamma_{\omega'}}\right)\\
&\quad\times\frac{C_{\gamma\rho'}}{g_{\rho_1}}\left(\frac{16}{3}\,\pi^2 m_u V_{\rho'}\right)\exp(i\pi),\\
T_{\phi'} &= -\frac{2\sqrt{2}}{3}\,\frac{s}{m_{\phi'}^2 - s - i\sqrt{s}\,\Gamma_{\phi'}}\,\frac{C_{\gamma\phi'}}{g_{\phi_1}}\left(\frac{16}{3}\,\pi^2 m_s V_{\phi'}\right).
\end{aligned} \tag{62}$$

The coefficients $C_{\gamma V}$ denote the constants of the transition of a virtual photon into a vector meson:

$$\begin{aligned}
C_{\gamma V} &= \frac{\sin(\beta^q + \beta_0^q)}{\sin(2\beta_0^q)} + R_V\,\frac{\sin(\beta^q - \beta_0^q)}{\sin(2\beta_0^q)}\,,\\
C_{\gamma V'} &= -\left[\frac{\cos(\beta^q + \beta_0^q)}{\sin(2\beta_0^q)} + R_V\,\frac{\cos(\beta^q - \beta_0^q)}{\sin(2\beta_0^q)}\right].
\end{aligned} \tag{63}$$

The values for vertices are taken in the low-momentum approximation:

$$\begin{aligned}
V_{\gamma q}^{\eta,\eta',\hat{\eta},\hat{\eta}'} &= \sum_{i=1,2} b_{\eta,\hat{\eta},\eta',\hat{\eta}'}^{\varphi_{q,i}}\, g_{q_i} I_3^{(0)}(m_q)\,,\\
V_{V_q}^{\eta,\eta',\hat{\eta},\hat{\eta}'} &= \frac{\sin(\beta^q + \beta_0^q)}{\sin(2\beta_0^q)}\, b_{\eta,\hat{\eta},\eta',\hat{\eta}'}^{\varphi_{q,1}}\, g_{V_1} g_{q_1} I_3^{(0)}(m_q)\\
&\quad + \frac{\sin(\beta^q - \beta_0^q)}{\sin(2\beta_0^q)}\, b_{\eta,\hat{\eta},\eta',\hat{\eta}'}^{\varphi_{q,1}}\, g_{V_2} g_{q_1} I_3^{(1)}(m_q)\\
&\quad + \frac{\sin(\beta^q + \beta_0^q)}{\sin(2\beta_0^q)}\, b_{\eta,\hat{\eta},\eta',\hat{\eta}'}^{\varphi_{q,2}}\, g_{V_1} g_{q_2} I_3^{(1)}(m_q)\\
&\quad + \frac{\sin(\beta^q - \beta_0^q)}{\sin(2\beta_0^q)}\, b_{\eta,\hat{\eta},\eta',\hat{\eta}'}^{\varphi_{q,2}}\, g_{V_2} g_{q_2} I_3^{(2)}(m_q)\,,\\
-V_{V_q'}^{\eta,\eta',\hat{\eta},\hat{\eta}'} &= \frac{\cos(\beta^q + \beta_0^q)}{\sin(2\beta_0^q)}\, b_{\eta,\hat{\eta},\eta',\hat{\eta}'}^{\varphi_{q,1}}\, g_{V_1} g_{q_1} I_3^{(0)}(m_q)\\
&\quad + \frac{\cos(\beta^q - \beta_0^q)}{\sin(2\beta_0^q)}\, b_{\eta,\hat{\eta},\eta',\hat{\eta}'}^{\varphi_{q,1}}\, g_{V_2} g_{q_1} I_3^{(1)}(m_q)\\
&\quad + \frac{\cos(\beta^q + \beta_0^q)}{\sin(2\beta_0^q)}\, b_{\eta,\hat{\eta},\eta',\hat{\eta}'}^{\varphi_{q,2}}\, g_{V_1} g_{q_2} I_3^{(1)}(m_q)\\
&\quad + \frac{\cos(\beta^q - \beta_0^q)}{\sin(2\beta_0^q)}\, b_{\eta,\hat{\eta},\eta',\hat{\eta}'}^{\varphi_{q,2}}\, g_{V_2} g_{q_2} I_3^{(2)}(m_q)\,.
\end{aligned} \tag{64}$$

The energy dependence of the ρ'-meson width can be taken into account using the formula

$$\begin{aligned}
\Gamma_{\rho'}(s) &= \Theta(2m_\pi - \sqrt{s})\,\Gamma_{\rho'\to 2\pi} + \Theta(\sqrt{s} - 2m_\pi)\\
&\quad\times\left(\Gamma_{\rho'\to 2\pi} + \Gamma_{\rho'\to\omega\pi}\,\frac{\sqrt{s} - 2m_\pi}{m_\omega - m_\pi}\right)\Theta(m_\omega + m_\pi - \sqrt{s})\\
&\quad + \Theta(m_{\rho'} - \sqrt{s})\,\Theta(\sqrt{s} - m_\omega - m_\pi)\\
&\quad\times\left[\Gamma_{\rho'\to 2\pi} + \Gamma_{\rho'\to\omega\pi} + (\Gamma_{\rho'} - \Gamma_{\rho'\to 2\pi} - \Gamma_{\rho'\to\omega\pi})\right.\\
&\quad\left.\times\,\frac{\sqrt{s} - m_\omega - m_\pi}{m_{\rho'} - m_\omega - m_\pi}\right] + \Theta(\sqrt{s} - m_{\rho'})\,\Gamma_{\rho'}\,,
\end{aligned} \tag{65}$$

where $\Gamma_{\rho'\to 2\pi} = 22$ MeV and $\Gamma_{\rho'\to\omega\pi} = 75$ MeV were obtained in [19], and $\Gamma_{\rho'} = 400$ MeV is the full width of the ρ' meson. We use full widths of the excited ω' and ϕ' mesons. This is justified by their small contributions compared to that from the ρ' meson. We note that the contribution from the ϕ' meson is noticeable only for energies $\sqrt{s} > 1.5$ GeV. Unfortunately, the ENJL model cannot predict the relative phases between the ground and excited states of the intermediate mesons, and we therefore choose them from the approximation of experimental data in the framework of the vector dominance model [39].

The total cross section of the considered process has the form

$$\sigma(s) = \frac{\alpha}{24\pi^2 s^3}\,\lambda^{3/2}(s, m, 0)\,|T|^2\,, \tag{66}$$

where $\lambda(a,b,c) = (a-b-c)^2 - 4bc$ and $m = m_\eta, m_{\eta'}, m_{\hat{\eta}}, m_{\hat{\eta}'}$. The results of numerical calculations are presented in Figs 7–10. Figure 7 also shows a comparison with experimental data [39]. Figures 8–10 show the ENJL model predictions. These figures suggest that accounting for the excited states is important at energies above 1 GeV. Our predictions can be

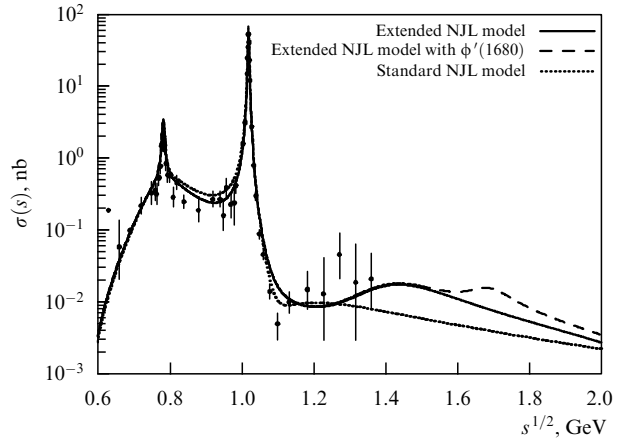

Figure 7. Comparison of the NJL model predictions with experimental data [39] for the process $e^+e^- \to \eta\gamma$.

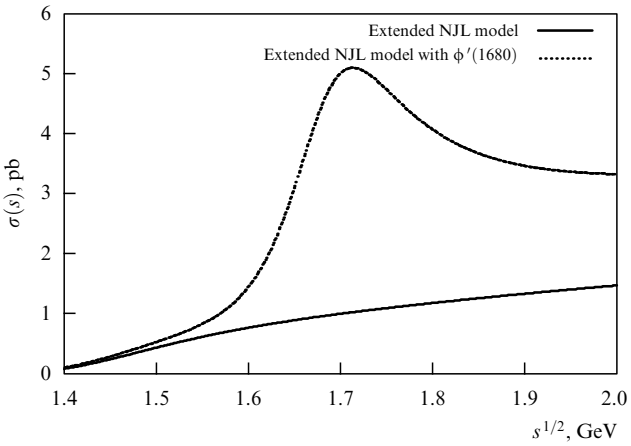

Figure 9. Predicted cross section of the process $e^+e^- \to \eta(1295)\gamma$ as a function of energy.

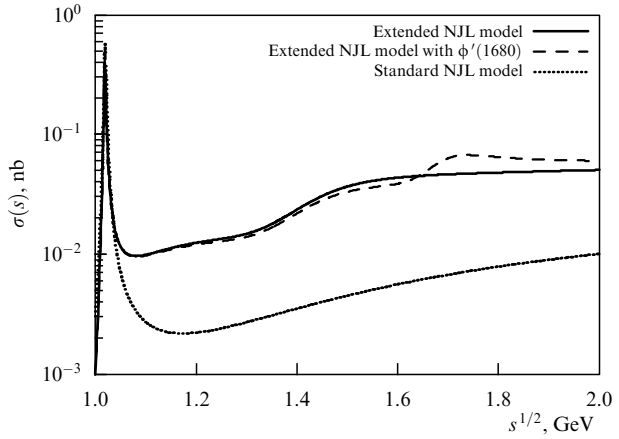

Figure 8. Predicted cross section of the process $e^+e^- \to \eta'\gamma$ as a function of energy.

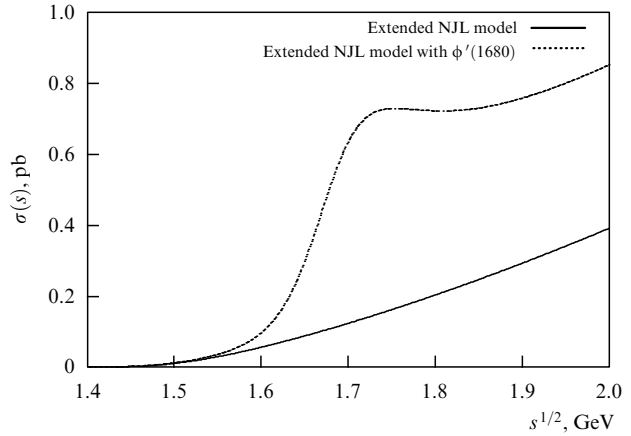

Figure 10. Predicted cross section of the process $e^+e^- \to \eta(1475)\gamma$ as a function of energy.

used to select the physical program of further experimental research on modern electron–positron colliders.

4.3 Process $e^+e^- \to \pi\omega$

The e^-e^+ annihilation into a $\omega\pi^0$ meson pair with subsequent $\omega \to \pi^0\gamma$ decay was studied at energies below 2 GeV in several experiments: DM2 (from the French Detecteur Magnetique 2) [41], ND (Neutral Detector) [42], and CMD-2 (Cryogenic Magnetic Detector) [44]. For a theoretical description of this process, several phenomenological models have been used, which are typically based on the chiral symmetry and vector dominance principles. A generalized vector dominance model with the contribution from the intermediate vector mesons $\rho(770)$, $\rho'(1450)$, and $\rho''(1700)$ was used in [44]. Arbitrary free parameters inferred from experimental data were introduced there. Earlier, the $\rho' \to \omega\pi$ decay was considered in the relativistic [45] and nonrelativistic [46] quark models. In [47], the $e^+e^- \to \omega\pi^0$ process was studied at energies near the ϕ-meson resonance, where experimental data obtained by the KLOE (K Long Experiment) collaboration [48] are available. Here, we do not focus on this energy range and ignore the contribution from the ϕ meson at energies above its mass (and below 2 GeV). We note that in [44, 49, 50], different models were used to show that the contribution from the second radially excited state $\rho''(1700)$ to this process is small. In the ENJL model, this process is described in [51, 52]. Unlike the models used in the papers cited above, our model does not require the use of any additional parameters.

Unlike the process $e^+e^- \to \pi\gamma$ discussed in Section 4.1, the process we consider here includes only $\rho^0(770)$ and $\rho'(1450)$ as the intermediate mesons (in addition to a photon). The amplitude of this process takes the form

$$T = \bar{e}\,\gamma_\mu e\,\frac{1}{s}\,\varepsilon_{\mu\lambda\nu\eta}\,p_\omega^\nu\,p_\pi^\eta\big(T_\gamma + T_\rho + T_{\rho'}\big)\epsilon_\lambda(\omega)\,, \tag{67}$$

where $s = (p_1(e^+) + p_2(e^-))^2 \equiv q^2$, and ϵ is the polarization vector of the ω meson. The amplitude calculation is fully analogous to that given in Section 4.2, with the only difference in the expression for the triangle vertex describing the $\pi\omega$ pair production instead of the $\pi\gamma$ pair. In particular, the $\rho \to \pi\omega$ transition vertex in the ENJL model is

$$\begin{aligned} V_{\rho\omega\pi} = g_{\pi_1}\Bigg\{ & g_{\rho_1}\left[\frac{\sin(\beta+\beta_0)}{\sin(2\beta_0)}\right]^2 I_3^{(0)}(m_u) \\ & + \frac{g_{\rho_2}^2}{g_{\rho_1}}\left[\frac{\sin(\beta-\beta_0)}{\sin(2\beta_0)}\right]^2 I_3^{(2)}(m_u) \\ & + 2g_{\rho_2}\,\frac{\sin(\beta+\beta_0)}{\sin(2\beta_0)}\,\frac{\sin(\beta-\beta_0)}{\sin(2\beta_0)}\,I_3^{(1)}(m_u)\Bigg\}. \end{aligned} \tag{68}$$

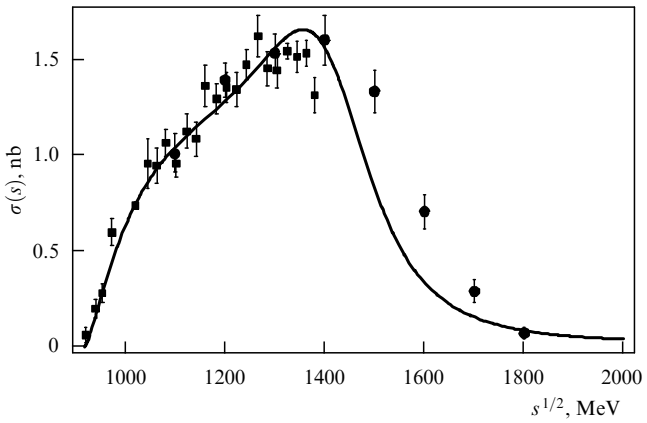

Figure 11. Comparison of the SND-2 experimental data (dark squares [43] and circles [53]) for the process $e^+e^- \to \pi\omega$ with the ENJL model predictions (solid curve).

The large number of terms in this vertex is due to the form factors in both the ρ-meson and ω-meson vertices. A detailed description of other vertices can be found in [52]. The obtained amplitudes enable the calculation of the energy dependence of this process, shown in Fig. 11. It can be seen that the predictions are compatible with the experimental data. Especially good agreement is observed at energies up to 1.4 GeV. At higher energies, contributions from higher-order excited states of the intermediate vector mesons should be taken into account for better agreement.

Similar calculations in the ENJL framework for the process $e^+ + e^- \to \pi^0 + \rho^0$ are presented in [54].

4.4 Process $e^+e^- \to \pi^+\pi^-$, $\pi\pi'$

The e^-e^+ annihilation into a pair of charged pions was carefully investigated both experimentally [55] (also see the references therein) and theoretically [56–61]. However, in most theoretical papers, additional parameters had to be introduced to satisfactorily describe the experimental data. At the same time, in the ENJL model, such a description can be obtained without introducing additional free parameters. This allows describing both the experimental data and theoretical predictions for the production of the charged π and $\pi'(1300)$ meson pairs.

To describe the $e^+e^- \to \pi^+\pi^-, \pi\pi'$ processes at energies below 1 GeV, it is sufficient to use the standard NJL model taking the intermediate states of the photon and ρ and ω mesons in the ground states into account. However, at higher energies, the intermediate state $\rho'(1450)$ becomes important. In the ENJL model, the first radially excited states of mesons for this process was taken into account in [62].

The $e^+e^- \to \pi^+\pi^-$ process amplitude is described by the diagrams shown in Figs 12 and 13. The amplitude is

$$T = \bar{e}\gamma_\mu e \frac{4\pi\alpha}{s}(B_\gamma + B_\rho + B_\omega + B_{\rho'}) f_{a_1}(s)(p^\mu_{\pi^+} - p^\mu_{\pi^-}), \quad (69)$$

where $\alpha \approx 1/137$, $s = (p_{e^+} + p_{e^-})^2$, and $f_{a_1}(s)$ describes the pion production through the intermediate a_1 mesons,

$$f_{a_1}(p^2) = \frac{1}{Z} + \left(1 - \frac{1}{Z}\right) + \left(\frac{p^2 - m_\pi^2}{(g_\rho F_\pi)^2}\right)^2 (1 - Z)$$
$$= 1 + \left(\frac{p^2 - m_\pi^2}{(g_\rho F_\pi)^2}\right)^2 (1 - Z), \quad (70)$$

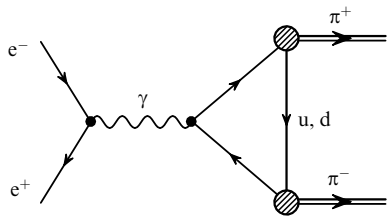

Figure 12. Contact diagram describing the creation of a pion pair by an intermediate photon.

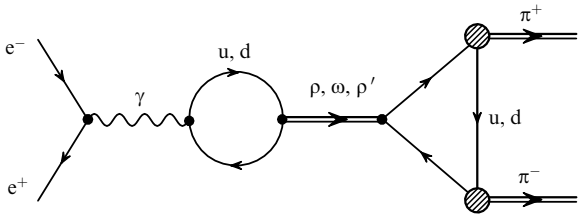

Figure 13. Diagram of the process $e^+e^- \to \pi^+\pi^-$ with intermediate vector mesons.

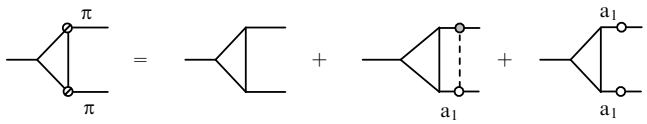

Figure 14. Diagram vertexes with $\pi - a_1$-transitions.

where Z is the renormalization factor described in Section 2.1 that takes the $\pi - a_1$ transitions into account. The first term describes production of two pions directly from the quark triangle loop, the second term corresponds to a situation where one of the pions is produced via the intermediate $a_1(1260)$ meson, and the third term describes both pions produced via the intermediate a_1 mesons (Fig. 14).

The contribution from the photon exchange diagram is normalized to unity: $B_\gamma = 1$. With the $\gamma - \rho$ transitions, the quantity B_ρ has the form

$$B_\rho = \frac{C_{\gamma\rho} C_{\rho\pi\pi}}{g_\rho} \frac{s}{m_\rho^2 - s - i\sqrt{s}\,\Gamma_\rho(s)},$$
$$C_{\gamma\rho} = \frac{\sin(\beta + \beta_0)}{\sin(2\beta_0)} + R_\rho \frac{\sin(\beta - \beta_0)}{\sin(2\beta_0)}. \quad (71)$$

The ρππ vertex is proportional to the coefficient

$$C_{\rho\pi\pi} = \frac{\sin(\beta + \beta_0)}{\sin(2\beta_0)} g_{\rho_1} + \frac{\sin(\beta - \beta_0)}{\sin(2\beta_0)} \frac{I_2^{(1)}}{I_2^{(0)}} g_{\rho_2}. \quad (72)$$

For the contribution from the intermediate ω meson, we obtain

$$B_\omega = \frac{C(s) C_{\rho\pi\pi} C_{\gamma\rho}}{3 g_\rho^2} \frac{s}{m_\omega^2 - s - i\sqrt{s}\,\Gamma_\omega(s)}, \quad (73)$$

where the function $C(s) = C_1(s) + C_2(s)$ describes the transition of the ω meson into a ρ meson with its subsequent decay into two pions. The function $C_1(s)$ describes the direct transition into the ρ meson due to the difference in the u and

d quarks,

$$C_1(s) = \frac{g_\rho^3 m_\omega^2}{3(m_\rho^2 - s - i\sqrt{s}\,\Gamma_\rho(s))}\,\frac{3}{(4\pi)^2}\,\ln\frac{m_d^2}{m_u^2}\,, \qquad (74)$$

and C_2 describes the contribution from the $\omega \to \gamma \to \rho$ transition:

$$C_2(s) = -\frac{4\pi\alpha\, s}{3g_\rho(m_\rho^2 - s - i\sqrt{s}\,\Gamma_\rho(s))}\,. \qquad (75)$$

The last part of the amplitude with intermediate ρ' mesons is similar to the contribution from the ρ-meson ground state:

$$B_{\rho'} = \exp(i\pi)\,\frac{C_{\gamma\rho'}C_{\rho'\pi\pi}}{g_\rho}\,\frac{s}{m_{\rho'}^2 - s - i\sqrt{s}\,\Gamma_{\rho'}(s)}\,,$$

$$C_{\gamma\rho'} = -\left[\frac{\cos(\beta+\beta_0)}{\sin(2\beta_0)} + R_\rho\,\frac{\cos(\beta-\beta_0)}{\sin(2\beta_0)}\right], \qquad (76)$$

$$C_{\rho'\pi\pi} = -\left[\frac{\cos(\beta+\beta_0)}{\sin(2\beta_0)}\,g_{\rho_1} + \frac{\cos(\beta-\beta_0)}{\sin(2\beta_0)}\,\frac{I_2^{(1)}}{I_2^{(0)}}\,g_{\rho_2}\right] = 1.68\,.$$

Unfortunately, the model we use does not allow determining the relative phase of amplitudes with intermediate ρ mesons in the ground and excited states. Guided by experimental data, we have chosen the phase difference equal to $\exp(i\pi)$. The energy dependence of the width $\Gamma_{\rho'}$ can be taken into account using a formula in [63].

For the total cross section, we obtain

$$\sigma(s) = \frac{\alpha^2\pi}{12s}\,f_{a_1}^2(s)\left(1 - \frac{4m_\pi^2}{s}\right)^{3/2}\left|B_\gamma + B_\rho + B_\omega + B_{\rho'}\right|^2. \qquad (77)$$

It can be seen from Fig. 15 that our results are in good agreement with experimental data [55] for the $e^+e^- \to \pi^+\pi^-$ process in the energy range up to 1 GeV.

In considering the $e^+e^- \to \pi\pi'$ process, it is possible to disregard the contribution from diagrams with an intermediate ω meson. The cross section, which is constructed in full analogy with the $\pi^+\pi^-$ pair creation, has the form

$$\sigma(s) = \frac{\alpha^2\pi}{12s^2}\,\Lambda^{3/2}(s, m_{\pi'}^2, m_\pi^2)\left|B_\gamma^{\pi\pi'} + B_\rho^{\pi\pi'} + B_{\rho'}^{\pi\pi'}\right|^2. \qquad (78)$$

Unlike the previous process, the considered process requires accounting for the contribution from the component with the

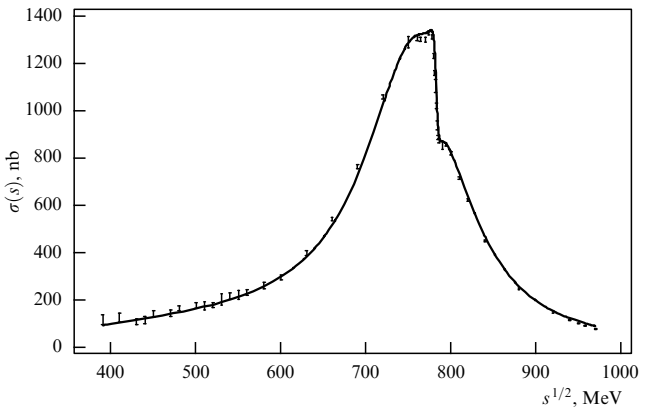

Figure 15. Comparison of the NJL model cross section with experimental data [55] for the process $e^+e^- \to \pi^+\pi^-$.

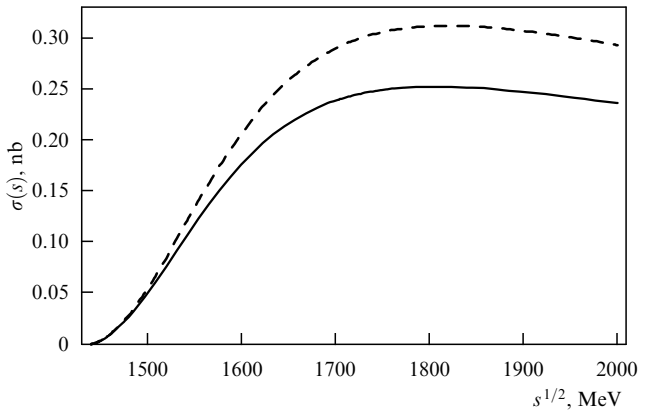

Figure 16. The ENJL model cross section for the process $e^+e^- \to \pi\pi'$. The respective solid and dashed curves show the total cross section and the contribution from the intermediate $\rho'(1450)$.

form factor also in the vertex with an outgoing $\pi'(1300)$ meson. The energy dependence of the $\pi'(1300)$ process cross section is presented in Fig. 16. Our results for this process are qualitative, because no contribution from the intermediate state of the second radially excited state of ρ(1700) has been taken into account.

4.5 Process $e^+e^- \to \eta(\eta')2\pi$

After the two-pion annihilation process studied in Section 4.4, it would be natural to consider the process $e^+e^- \to 3\pi$. It can be easily described following [64], where the 'subprocess' $\gamma^* \to 3\pi$ with the intermediate ω-meson contribution is described in detail in the framework of the chiral-symmetric model. Therefore, we restrict ourselves here to referencing this paper and immediately turn to describing a more interesting annihilation process into three pseudoscalars with participation of the η or η' mesons.

We conclude our discussion of the meson production processes in colliding e^-e^+ beams by considering the reactions

$$e^+ + e^- \to \eta(\eta') + \pi^+ + \pi^-\,,$$

which are also mediated by the intermediate ρ and ρ' mesons. These processes have been studied experimentally in a number of experiments, including DM1 [65], DM2 [66], ND [42, 67], CMD-2 [68], and BaBar [69]. From the theoretical standpoint, these processes have been discussed using different phenomenological models [68, 70, 71]. Here, we present calculations [72] of these processes in the ENJL model and compare them with the experimental and theoretical results obtained in the theoretical papers cited above.

The full amplitude of the considered process is

$$T = -\frac{4\pi\alpha}{q^2}\,\bar{e}\,\gamma^\mu e\,\mathcal{H}_\mu\,, \qquad (79)$$

where $q = p_{e^+} + p_{e^-}$ in the center-of-mass reference frame. The hadronic part of the amplitude includes contributions from the intermediate photon and vector ρ and ρ' mesons (here, $\boldsymbol{\eta} = \eta, \eta'$):

$$\mathcal{H}_\mu = V_\mu\left(T_\gamma(q^2, s) + \sum_{V=\rho,\,\rho'} T_V(q^2, s)\right),$$
$$V_\mu = p_{\boldsymbol{\eta}}^\alpha\, p_{\pi^+}^\beta\, p_{\pi^-}^\gamma\, \varepsilon_{\mu\alpha\beta\gamma}\,. \qquad (80)$$

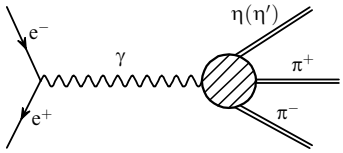

Figure 17. Feynman diagram with an intermediate photon. The dashed circle denotes the sum of two subdiagrams shown in Figs 19 and 20.

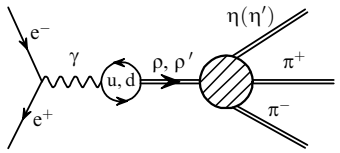

Figure 18. Feynman diagram with intermediate vector mesons ρ(770) and ρ(1450).

The corresponding Feynman diagrams are presented in Figs 17 and 18 with the contributions

$$
\begin{aligned}
T_\gamma(q^2,s) &= \sum_{i=1}^{2} g_{\pi_i}\chi_{\boldsymbol{\eta}}^{i}\bigl(T_{\square}^{(i-1)}(s)+T_{\triangle}^{(i-1)}(s)\bigr)\,,\\
T_V(q^2,s) &= \frac{(C_{\gamma V}/g_{V_1})q^2}{m_V^2-q^2-\mathrm{i}\sqrt{q^2}\,R\Gamma_V(q^2)}\\
&\quad\times\sum_{i=1}^{2}\sum_{j=1}^{2} g_{\pi_i}\chi_{\boldsymbol{\eta}}^{i}g_{V_j}\chi_V^{j}\bigl(T_{\square}^{(i+j-2)}(s)+T_{\triangle}^{(i+j-2)}(s)\bigr)\,.
\end{aligned}
\tag{81}
$$

To simplify the formulas, we introduce the notation for frequently encountered mixing angle combinations:

$$
\begin{aligned}
\chi_\pi &= \frac{1}{\sin(2\alpha_0)}\begin{pmatrix}\sin(\alpha+\alpha_0)\\ \sin(\alpha-\alpha_0)\end{pmatrix},\\
\chi_\eta &= \begin{pmatrix}0.71\\ 0.11\end{pmatrix},\quad \chi_{\eta'}=\begin{pmatrix}-0.32\\ -0.48\end{pmatrix},\\
\chi_\rho &= \frac{1}{\sin(2\beta_0)}\begin{pmatrix}\sin(\beta+\beta_0)\\ \sin(\beta-\beta_0)\end{pmatrix},\\
\chi_{\rho'} &= -\frac{1}{\sin(2\beta_0)}\begin{pmatrix}\cos(\beta+\beta_0)\\ \cos(\beta-\beta_0)\end{pmatrix}.
\end{aligned}
\tag{82}
$$

The vertices $\gamma\boldsymbol{\eta}\pi\pi$ and $V\boldsymbol{\eta}\pi\pi$ contain two contributions:

$$
\begin{aligned}
T_{\square}^{(n)}(s) &= -24F_\pi g_\pi^3 I_4^{(n)}\,,\\
T_{\triangle}^{(n)}(s) &= 16F_\pi g_\pi \sum_{V=\rho,\rho'}\frac{g_{V\to\pi\pi}}{m_V^2-s-\mathrm{i}\sqrt{s}\,\Gamma_V(s)}\\
&\quad\times\sum_{i=1}^{2} g_{\rho_i}\chi_V^{i} I_3^{(n+i-1)}\\
&\approx 16F_\pi g_\pi\,\frac{g_{\rho\to\pi\pi}}{m_\rho^2-s-\mathrm{i}\sqrt{s}\,\Gamma_\rho(s)}\sum_{i=1}^{2} g_{\rho_i}\chi_\rho^{i} I_3^{(n+i-1)}\,.
\end{aligned}
\tag{83}
$$

The $T_{\square}^{(n)}(s)$ contribution corresponds to the so-called anomalous quark diagram (see Fig. 19). The contribution $T_{\triangle}^{(n)}(s)$ originates from two triangle quark loops connected by a virtual vector meson (see Fig. 20). We have ignored the intermediate ρ(1450) meson contribution to $T_{\triangle}^{(n)}(s)$ because it is strongly suppressed compared to the ρ(770) contribution

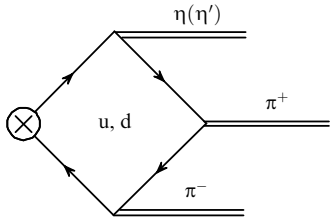

Figure 19. Vertex subdiagram $V\eta\pi\pi$ with a box quark loop.

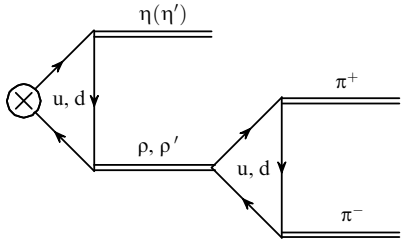

Figure 20. Vertex subdiagram $V\eta\pi\pi$ with two triangle quark loops.

due to the kinematics and the small partial width of the ρ(1450) → 2π decay (see [19]).

Because $g_{\pi_1}\chi_\pi^1 \gg g_{\pi_2}\chi_\pi^2 \approx 0$, we disregard the contributions with the form factor at pion vertices, as in calculations of other processes:

$$
\prod_{i=1}^{n}\sum_{j=1}^{2} g_{\pi_j}\chi_\pi^{j} T_{\text{non}-\pi}^{(k)} I_{n+k}^{(k+ij-i)}\Bigg|_{g_{\pi_2}\chi_\pi^2\to 0} = g_{\pi_1}^{n}\,T_{\text{non}-\pi}^{(k)} I_{n+k}^{(k)}\,.
$$

The second triangle diagram shown in Fig. 20 was calculated in the ENJL model in [19]:

$$
g_{V\to\pi\pi} \approx g_{\rho_1}\chi_V^1 + g_{\rho_2}\chi_V^2\,\frac{I_2^{(1)}}{I_2^{(0)}}\,. \tag{84}
$$

The photon-to-vector-meson (ρ, ρ′) transition is described by the factor

$$
C_{\gamma V} = \chi_V^1 + \chi_V^2\,\frac{I_2^{(1)}}{\sqrt{I_2^{(0)}I_2^{(2)}}}\,. \tag{85}
$$

Here, we use the fixed width $\Gamma_\rho = 147.8$ MeV for the ρ(770) ground state and the energy-dependent width for ρ(1450) according to formula (65).

The total cross section of the process is

$$
\sigma(q^2) = \frac{\alpha^2}{192\pi q^6}\int_{s_-}^{s_+}\mathrm{d}s\int_{t_-}^{t_+}\mathrm{d}t\,\bigl|T(q,s,t)\bigr|^2\,, \tag{86}
$$

where $s=(p_{\boldsymbol{\eta}}+p_{\pi^+})^2$, $t=(p_{\boldsymbol{\eta}}+p_{\pi^-})^2$, and the integration limits are defined as

$$
\begin{aligned}
t_\mp &= \frac{1}{4s}\Bigl([q^2+m_{\boldsymbol{\eta}}^2-2m_\pi^2]^2\\
&\quad-\bigl[\lambda^{1/2}(q^2,s,m_\pi^2)\pm\lambda^{1/2}(m_{\boldsymbol{\eta}}^2,m_\pi^2,s)\bigr]^2\Bigr)\,,\\
s_- &= (m_{\boldsymbol{\eta}}+m_\pi)^2\,,\qquad s_+=\bigl(\sqrt{q^2}-m_\pi\bigr)^2\,,\\
\lambda(a,b,c) &= (a-b-c)^2-4bc\,.
\end{aligned}
\tag{87}
$$

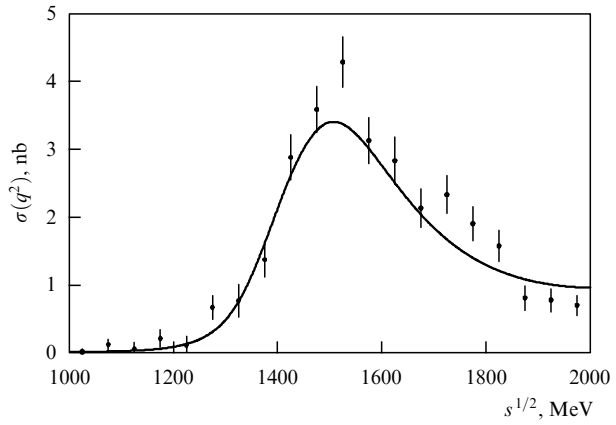

Figure 21. Comparison of the ENJL model predictions with experimental results of the BaBar collaboration [69] for the process $e^+e^- \to \eta 2\pi$.

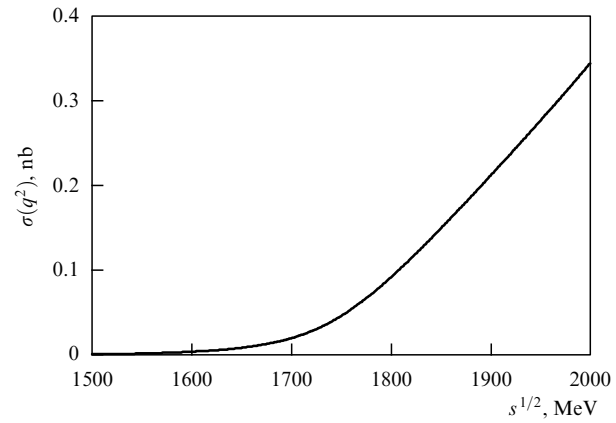

Figure 22. The ENJL model cross section for the process $e^+e^- \to \eta' 2\pi$.

Numerical results for the energy dependence of the cross section are presented in Figs 21 and 22.

The obtained results suggest that the ENJL model allows a description of the energy dependence of the total cross section of the $e^+e^- \to \eta 2\pi$ process in good agreement with experimental data below 2 GeV. This enables us to suppose that predictions obtained for the $e^+e^- \to \eta' 2\pi$ process are reasonable in the same energy range.

One of the first theoretical attempts to describe experimental data for the $e^+e^- \to \eta 2\pi$ process is presented in [68], where a generalized vector dominance model with the intermediate $\rho(770)$, $\rho(1450)$, and $\rho(1700)$ mesons was used. We note that several additional free parameters were introduced there, which were then fitted to experimental data. In addition, only the structure with two triangle diagrams was taken into account. It is also important to note that the fitting to experimental data suggested a negligibly small numerical contribution from the second radially excited state of $\rho(1700)$.

In [70], a model based on the resonance chiral symmetry was used. This model also contains a large number of free parameters. However, the intermediate state of the $\rho(1450)$ meson, which clearly plays a significant role in the considered energy range, was neglected in [70]. Later, in [71], the intermediate states of the $\rho(770)$, $\rho(1450)$, and $\rho(1700)$ mesons with additional free parameters were taken into account. The results in [71] also showed that the contribution due to $\rho(1700)$ is insignificant.

5. Tau-lepton decays

The ENJL model also allows describing the leading semi-lepton modes of τ-lepton decays. We emphasize that here we can also avoid introducing arbitrary parameters. The mechanism of constructing the amplitudes of these decays is very similar to the one we used for cross sections of electron–position annihilation processes with production of mesons at low energies described in Section 4. The role of the intermediate photons in the τ-lepton decays is played by $W^{\pm}$ bosons, which can generate charged intermediate vector mesons in both the ground and radially excited states.

Importantly, because the mass of the τ lepton is 1777 MeV, the role of the second and higher radially excited intermediate states here is quite insignificant. Therefore, it is possible to expect that the ENJL model, which takes only the ground and first radially excited states of mesons into account, should give very satisfactory theoretical predictions for the leading semi-lepton modes of the τ-lepton decays. In Sections 5.1–5.7, we consider a range of the main decay modes of τ-leptons and check the model assumptions.

5.1 Decay $\tau^- \to \pi^-(\pi^-(1300))\nu_\tau$

We start by considering the simplest mode of the semi-lepton $\tau^- \to \pi^-\nu_\tau$ decay and describing a similar process producing the first radially excited pion state $\tau^- \to \pi^-(1300)\nu_\tau$. We note that besides the decay width calculation, of interest is also the determination of the weak decay constants F_π and $F_{\pi'}$, which play an important role in constructing different chiral models in meson physics.

To describe the τ-lepton decays, in addition to the quark–meson Lagrangian, we need the Lagrangian of the weak coupling of the lepton current to quarks:

$$\mathcal{L}^{\text{weak}} = \bar{\tau}\gamma_\mu\gamma_5 \nu \, \frac{G_F}{\sqrt{2}} \, |V_{ud}| \bar{d}\gamma_5\gamma_\mu u \,, \tag{88}$$

where $G_F = 1.1663787(6) \times 10^{-5}$ GeV^{-2} is the Fermi constant and $|V_{ud}| = 0.97425(22)$ is the Cabbibo–Kobayashi–Maskawa matrix element. Only the axial part of the currents is written here because the production of a pseudoscalar pion is considered.

First, we calculate the $\tau \to \pi\nu_\tau$ decay width in the standard NJL model. The corresponding quark–meson Lagrangian has the form

$$\begin{aligned} &\mathcal{L} = \bar{q}\left[\tau^-\gamma_5(ig_\pi\pi^- + \gamma_\mu a_{1\mu}^-)\right]q \,, \\ &\tau^- = \sqrt{2}\begin{pmatrix} 0 & 1 \\ 0 & 0 \end{pmatrix}. \end{aligned} \tag{89}$$

The one-loop Feynman diagram (Fig. 23) is the main contributor to this process. The corresponding amplitude is

$$A_{\tau\to\pi\nu_\tau} = \frac{G_F}{\sqrt{2}} \, L_\mu |V_{ud}| H_\mu \,, \tag{90}$$

where $L_\mu = \bar{u}_\nu\gamma_\mu\gamma_5 u_\tau$ is the lepton current and H_μ is the hadron current. In the one-loop approximation (see Fig. 23), the hadron current is given by

$$H_\mu^{(1)} = p^\mu \sqrt{2}\, g_{\pi_1} 4 m_u \, I_2^{(0)}(m_u) = p^\mu \sqrt{2} \, \frac{m_u}{Z g_{\pi_1}} \,. \tag{91}$$

To obtain the final expression, it is necessary to consider the two-loop approximation with an intermediate a_1 meson

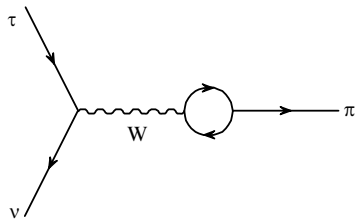

Figure 23. Feynman diagram for the one-loop contribution to the $\tau \to \pi\nu_\tau$ decay.

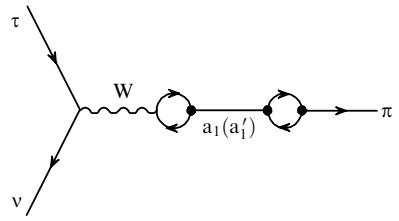

Figure 24. Diagram of the $\tau \to \pi\nu_\tau$ decay with an intermediate axial-vector meson.

(Fig. 24). The two-loop approximation yields the following contribution to the hadron current amplitude:

$$H_\mu^{(2)} = p^\mu \sqrt{2}\,\frac{m_\mathrm{u}}{g_{\pi_1}}\left(1-\frac{1}{Z}\right). \tag{92}$$

The sum of the contributions to the hadron current yields

$$H_\mu = p^\mu \sqrt{2}\,\frac{m_\mathrm{u}}{g_{\pi_1}} = p^\mu \sqrt{2}\,F_\pi \tag{93}$$

in agreement with the Goldberger–Treiman relation ($g_\pi = m_\mathrm{q} F_\pi$). We recall that above we obtained $F_\pi \approx 92.8$ MeV from this relation. Then the theoretical value of the considered decay width $\Gamma^{\mathrm{theor}}(\tau \to \pi\nu) = 2.45 \times 10^{-10}$ MeV agrees with the experimental value $\Gamma^{\exp}(\tau \to \pi\nu) = 2.46(1) \times 10^{-10}$ MeV [27].

Similar calculations can also be performed in the ENJL model. For decays with the production of the ground state of a pion, contributions with form factors only at vertices with axial-vector mesons $a_1(1260)$ and $a_1'(1640)$ should be taken into account. The contribution from the first diagram has the same form (90), (91) as in the standard NJL model. The contribution from the intermediate $a_1(1260)$ meson to the hadron current takes the form

$$H_\mu^{(a_1)} = -\frac{6m_\mathrm{u}^2}{m_{a_1}^2}\sqrt{2}Z\,\frac{m_\mathrm{u}}{g_{\pi_1}}\,p^\mu\left[\frac{\sin(\beta+\beta_0)}{\sin(2\beta_0)} + R_V\frac{\sin(\beta-\beta_0)}{\sin(2\beta_0)}\right]^2. \tag{94}$$

The first radially excited state $a_1'(1640)$ yields

$$H_\mu^{(a_1')} = -\frac{6m_\mathrm{u}^2}{m_{a_1'}^2}\sqrt{2}Z\,\frac{m_\mathrm{u}}{g_{\pi_1}}\,p^\mu\left[\frac{\cos(\beta+\beta_0)}{\sin(2\beta_0)} + R_V\frac{\cos(\beta-\beta_0)}{\sin(2\beta_0)}\right]^2. \tag{95}$$

We have disregarded the pion mass in the denominator of the Breit–Wigner propagators because it is small compared to the a_1- and a_1'-meson masses.

In the ENJL model, three diagrams contribute to the decay constant F_π:

$$F_\pi^{\mathrm{ext}} = \frac{m_\mathrm{u}}{Zg_{\pi_1}}\left\{1 - \frac{6m_\mathrm{u}^2}{m_{a_1}^2}\left[\frac{\sin(\beta+\beta_0)}{\sin(2\beta_0)} + R_V\frac{\sin(\beta-\beta_0)}{\sin(2\beta_0)}\right]^2 - \frac{6m_\mathrm{u}^2}{m_{a_1'}^2}\left[\frac{\cos(\beta+\beta_0)}{\sin(2\beta_0)} + R_V\frac{\cos(\beta-\beta_0)}{\sin(2\beta_0)}\right]^2\right\}. \tag{96}$$

The estimate we obtain in the extended model, $F_\pi^{\mathrm{ext}} \approx 94.6$ MeV, is in satisfactory agreement with the standard value of the pion weak decay constant. This makes it possible to obtain reasonable estimates of the $\tau \to \pi'(1300)\nu$ decay width and the decay constant $F_{\pi'}$.

In the diagram shown in Fig. 23, an excited state of π' is present in the final state. The corresponding part of the hadron current takes the form

$$H_\mu^{\pi'} = p^\mu\sqrt{2}\,\frac{m_\mathrm{u}}{Zg_{\pi_1}}\left[\frac{\cos(\alpha+\alpha_0)}{\sin(2\alpha_0)} + R_\pi\,\frac{\cos(\alpha-\alpha_0)}{\sin(2\alpha_0)}\right]. \tag{97}$$

For a two-loop diagram like the one shown in Fig. 24, vertices describing the transition of a W boson into a_1 and a_1' have the same form as in the process with pion production in the ground state. Here, the widths should be taken into account in propagators of the a_1 and a_1' mesons:

$$B = \frac{1}{M_{a_1(a_1')}^2 - M_{\pi'}^2 - \mathrm{i}M_{a_1(a_1')}\Gamma_{a_1(a_1')}}\,. \tag{98}$$

In the vertices describing transitions of a_1 and a_1' into π', form factors in both the first and second quark loop vertices should be taken into account (see [73] for more details).

As a result, for the $\tau \to \pi'(1300)\nu_\tau$ decay width, we obtain $\Gamma^{\mathrm{total}}_{\tau\to\pi'\nu_\tau} = 2.2 \times 10^{-13}$ MeV. This value is consistent with the experimental estimate of this width reported in [74]: 2.27×10^{-13} MeV $< \Gamma^{\exp}_{\tau\to(\pi')\nu_\tau} < 4.31 \times 10^{-13}$. The decay width we obtain corresponds to the decay constant of the excited pion $F_{\pi'} = 4.7$ MeV.

5.2 Decay $\tau^- \to \pi^-\pi^0\nu_\tau$

The $\tau^- \to \pi^-\pi^0\nu_\tau$ decay is structurally very close to the pion pair production in electron–position annihilation considered in Section 4.4; only the weak interaction is used instead of the electromagnetic interaction, and a W boson plays the role of the intermediate photon (see Figs 12 and 13).

Here, we restrict ourselves to the case of pair production of pions in the ground state but with the contribution from intermediate ρ^- mesons in both the ground and first radially excited states taken into account (see [75, 76]). The amplitude of the considered decay is

$$T = G_\mathrm{F}|V_{\mathrm{ud}}|f_{a_1}(p^2)m_\rho^2\left[\frac{1-\mathrm{i}\sqrt{q^2}\Gamma_\rho(p^2)/m_\rho^2}{m_\rho^2 - p^2 - \mathrm{i}\sqrt{p^2}\Gamma_\rho(p^2)} + \frac{\exp(\mathrm{i}\pi)C_{\mathrm{W}\rho'}C_{\rho'\pi\pi}(1/g_\rho)p^2/m_\rho^2}{m_{\rho'}^2 - p^2 - \mathrm{i}\sqrt{p^2}\Gamma_{\rho'}(p^2)}\right](p_{\pi^-}^\mu - p_{\pi^0}^\mu)l_\mu\pi^-\pi^0, \tag{99}$$

where l_μ is the standard lepton current, and the form factor $f_{a_1}(p^2)$ of the ρ-meson decay into two pions is taken in accordance with formula (70). The factors

$$C_{\mathrm{W}\rho'} = -\left[\frac{\cos(\beta+\beta_0)}{\sin(2\beta_0)} + R_\rho\,\frac{\cos(\beta-\beta_0)}{\sin(2\beta_0)}\right], \tag{100}$$

$$C_{\rho'\pi\pi} = -\left[\frac{\cos(\beta+\beta_0)}{\sin(2\beta_0)}\,g_{\rho_1} + \frac{\cos(\beta-\beta_0)}{\sin(2\beta_0)}\,\frac{I_2^{(1)}}{I_2^{(0)}}\,g_{\rho_2}\right]$$

describe the mixing between the ground and excited states of vector mesons in the ENJL model. When taking the excited intermediate ρ(1450) into account, the phase coefficient $\exp(i\pi)$ is chosen to be the same as in the case of e^-e^+ annihilation. In the standard NJL model, vector dominance automatically arises after summation of the contributions from the contact diagram and the intermediate vector meson ρ(770). This determines the form of the first term in the square brackets in formula (99). The second term corresponds to the contribution from the intermediate radially excited vector meson ρ(1450) in the ENJL model.

As a result, we obtain a numerical estimate of the partial decay width $\mathrm{Br}(\tau^- \to \pi^-\pi^0\nu_\tau) = 24.8\%$, which is in satisfactory agreement with the experimental data (Table 6).

The relative contribution of the excited ρ(1450) meson is traditionally estimated using the phenomenological Kuhn–Santamaria parameterization proposed in [57]:

$$\frac{1}{1+\beta}\left(\frac{m_\rho^2}{m_\rho^2 - p^2 - i\sqrt{p^2}\Gamma_\rho(p^2)} + \beta\,\frac{m_{\rho'}^2}{m_{\rho'}^2 - p^2 - i\sqrt{p^2}\Gamma_{\rho'}(p^2)}\right). \quad (101)$$

The parameter β is found by fitting it to experimental data. We note that in the ENJL model, this parameter can be calculated and turns out to be dependent on the transferred momentum. Near the peak for $p^2 = m_{\rho'}^2$, we obtain

$$\beta \approx \exp(i\pi)\,\frac{C_{W\rho'}C_{\rho'\pi\pi}}{g_\rho} \approx -0.086\,. \quad (102)$$

This value is in agreement with estimates inferred from the experimental data [77–79] (see Table 6).

We note that the contribution to this decay from the first radially excited intermediate meson ρ′ is small. Indeed, the calculation of the partial width ignoring the ρ′ meson yields 24.7%.

5.3 Decay $\tau^- \to \eta(\eta')\pi^-\nu_\tau$

The decays $\tau^- \to \eta\pi^-\nu_\tau$ and $\tau^- \to \eta'\pi^-\nu_\tau$ have not been well studied experimentally so far; only upper limits on their partial widths are available [80]. Nevertheless, some theoretical papers make predictions in the frameworks of different phenomenological models [81–89]. These processes are interesting because they relate to so-called second-class decays, which are suppressed compared with the main hadron modes of the τ-lepton decay.

In the ENJL model (see [81]), the vector and scalar channels shown in Figs 25 and 26 make the greatest contribution to the amplitude of these processes. The vector channel contribution is

$$T_V = A_{\pi\eta(\eta')}m_\rho^2\left[\left(1 - \frac{i\sqrt{q^2}\Gamma_\rho(p^2)}{m_\rho^2}\right)\mathrm{BW}_\rho(p^2) + \beta_\rho\,\frac{p^2}{m_\rho^2}\,\mathrm{BW}_{\rho'}(p^2)\right](p^\mu_{\pi^-} - p^\mu_{\eta(\eta')})l_\mu\pi^-\eta(\eta')\,, \quad (103)$$

where $\mathrm{BW}_{\rho(\rho')}(p^2)$ is the Breit–Wigner propagator of the ρ mesons. The parameter β_ρ defines the relative contribution of the excited state ρ(1450); we take its value from Section 5.2, where the $\tau \to \pi\pi\nu_\tau$ decay width was calculated. Here, we use the possibility of the transition $\pi^0 \to \eta$ via a quark loop. This transition was calculated in [81]. Such transitions were first considered in [8] when calculating the $\omega \to \pi\pi$ decay width, which occurs due to the $\omega \to \rho^0$ transitions via a quark loop. Such transitions are possible due to the mass difference between the u and d quarks. The amplitude of the $\pi^0 \to \eta(\eta')$ transitions is

$$A_{\pi\eta(\eta')} = 2g_\pi^2\Big[\big(2I_1^{(0)}(m_\mathrm{d}) + m_{\eta(\eta')}^2 I_2^{(0)}(m_\mathrm{d})\big) - \big(2I_1^{(0)}(m_\mathrm{u}) + m_{\eta(\eta')}^2 I_2^{(0)}(m_\mathrm{u})\big)\Big]\frac{\epsilon_{\eta(\eta')}}{m_\pi^2 - m_{\eta(\eta')}^2}\,. \quad (104)$$

The constituent quark masses $m_\mathrm{u} = 280$ MeV and $m_\mathrm{d} = 283.7$ MeV are taken from calculations in [8], where these values were used to describe both the decay $\omega \to 2\pi$ and the mass difference between charged and neutral pions and kaons. The factors $\epsilon_\eta = \sin\bar\theta$ and $\epsilon_{\eta'} = \cos\bar\theta$ are expressed through the difference between mixing angles of the η mesons, $\bar\theta \approx 54^\circ = \theta_0 - \theta$, where $\theta_0 \approx 35.3^\circ$ is the ideal mixing angle and $\theta \approx -19^\circ$ describes the deviation from it.

A comparison of the transition constants $\pi \to \eta(\eta')$ with those found in [87, 88] is presented in Table 7.

Disregarding the scalar channel contribution, it is possible to obtain the following values for the partial widths of the considered decays:

$$\mathrm{Br}_V(\tau \to \eta\pi\nu) = 4.35 \times 10^{-6}\,, \quad (105)$$

$$\mathrm{Br}_V(\tau \to \eta'\pi\nu) = 1.11 \times 10^{-8}\,. \quad (106)$$

Table 6. Comparison of the partial width $\mathrm{Br}(\tau^- \to \pi^-\pi^0\nu_\tau)$ with experimental data.

	$\mathrm{Br}(\tau^- \to \pi^-\pi^0\nu_\tau)$, %	β
CLEO [77]	25.32 ± 0.15	-0.108 ± 0.007
Aleph [78]	$25.471 \pm 0.097 \pm 0.085$	-0.097 ± 0.006
Belle [79]	$25.24 \pm 0.01 \pm 0.39$	$-0.15 \pm 0.05^{+0.15}_{-0.04}$
Theory	24.8	−0.086

Table 7. Comparison of constants $\epsilon_{\pi\eta(\eta')}$.

$\lvert\epsilon_{\pi\eta}^{\mathrm{PR}}\rvert$ [87]	$\lvert\epsilon_{\pi\eta}^{\mathrm{NJL}}\rvert$ [81]	$\lvert\epsilon_{\pi\eta'}^{\mathrm{PR}}\rvert$ [88]	$\lvert\epsilon_{\pi\eta'}^{\mathrm{NJL}}\rvert$ [81]
1.34×10^{-2}	1.55×10^{-2}	$(3 \pm 1) \times 10^{-3}$	6.79×10^{-3}

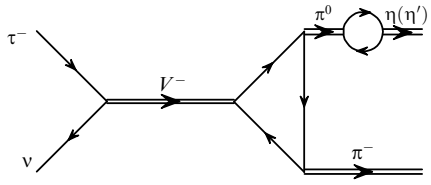

Figure 25. Feynman diagram with intermediate mesons $V^- = \rho^-(770)$, $\rho^-(1450)$.

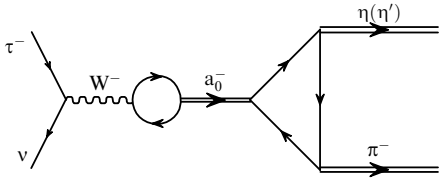

Figure 26. Feynman diagram with intermediate scalar mesons $a_0^-(980)$ or $a_0^-(1450)$.

The contributions from the intermediate scalar mesons $a_0^-(980)$ and $a_0^-(1450)$ are described by the diagram shown in Fig. 26. The transition $W^- \to a_0^-$ yields

$$\frac{\sqrt{3}}{4g_\rho}\, g_{EW}|V_{ud}|(m_d - m_u)\, p^\mu W_\mu^- a_0^- , \qquad (107)$$

where g_{EW} is the electroweak coupling constant. For the transition into the excited state $a_0^-(1450)$, we obtain

$$C_{Wa_0'} = \frac{\sqrt{3}}{4g_\rho}\, g_{EW}|V_{ud}|(m_d - m_u) \times \left[\frac{\cos(\phi+\phi_0)}{\sin(2\phi_0)} + R_\rho \frac{\cos(\phi-\phi_0)}{\sin(2\phi_0)}\right] p^\mu W_\mu^- a_0'^- , \qquad (108)$$

where we use the mixing angles for the scalar isovector mesons $\phi_0 = 65.5^\circ$ and $\phi = 72.0^\circ$.

The scalar channel amplitude is

$$T_S = 2Zm_u(m_d - m_u)\epsilon_{\eta(\eta')} \times \left(BW_{a_0}(p^2) + \beta_{a_0\eta(\eta')\pi} BW_{a_0'}(p^2)\right) p^\mu l_\mu \pi^-\eta(\eta') , \qquad (109)$$

where $BW_{a_0(a_0')}(p^2)$ is the Breit–Wigner propagator of scalar mesons. The masses and decay widths $m_{a_0} = 980$ MeV, $m_{a_0'} = 1474$ MeV, $\Gamma_{a_0'}(m_{a_0'}) = 265$ MeV are taken from [27], and the width $\Gamma_{a_0}(m_{a_0}) = 100$ MeV for the $a_0 \to \eta\pi$ decay is calculated in our model and corresponds to the upper bound of the range reported in [27]. The factor $\beta_{a_0\eta(\eta')\pi}$ is defined as

$$\beta_{a_0\eta(\eta')\pi} = \exp(i\pi) C_{Wa_0'} \frac{\sqrt{6}}{4Z} \frac{A_{a_0'\to\eta(\eta')\pi}}{m_u} , \qquad (110)$$

where we again use the relative phase $\exp(i\pi)$ for the excited meson contribution. We obtain $\beta_{a_0\eta\pi} = -0.24$ and $\beta_{a_0\eta'\pi} = -0.26$, which are close to the values found from fitting to the experimental data in [86, 88].

Considering only the scalar channel contributions, we obtain the partial widths

$$Br_S(\tau \to \eta\pi\nu) = 0.37 \times 10^{-6} , \qquad (111)$$

$$Br_S(\tau \to \eta'\pi\nu) = 2.63 \times 10^{-8} . \qquad (112)$$

We note that the obtained values for the scalar channel contributions are significantly smaller than those in [86, 88].

The full width of the considered decay can be expressed as

$$\Gamma = \frac{G_F^2|V_{ud}|^2}{384\pi m_\tau^2} \int_{m^2_{\eta(\eta')}+m_\pi^2}^{m_\tau^2} \frac{ds}{s^3}\, \lambda^{1/2}(s, m^2_{\eta(\eta')}, m_\pi^2)(m_\tau^2 - s)^2 \times \left(|T_V|^2(2s + m_\tau^2)\lambda(s, m^2_{\eta(\eta')}, m_\pi^2) + |T_S|^2 3m_\tau^2 (m^2_{\eta(\eta')} - m_\pi^2)^2\right) . \qquad (113)$$

We note that there is no interference here between the vector and scalar channel amplitudes. Therefore, the resulting partial widths are equal to the sum of the corresponding contributions:

$$Br(\tau^- \to \eta\pi^-\nu) = 4.72 \times 10^{-6} , \qquad (114)$$

$$Br(\tau^- \to \eta'\pi^-\nu) = 3.74 \times 10^{-8} . \qquad (115)$$

Interestingly, for a decay with the production of η', the scalar channel makes the leading contribution, dominated by the excited intermediate $a_0(1450)$ meson.

Table 8. The $\tau^- \to \eta(\eta')\pi^-\nu_\tau$ decay width in various models.

$\tau^- \to \eta\pi^-\nu_\tau$			
$Br_V \times 10^5$	$Br_S \times 10^5$	$Br_{S+V} \times 10^5$	References
0.25	1.60	1.85	[82]
0.12	1.38	1.50	[83]
0.15	1.06	1.21	[84]
0.36	1.00	1.36	[85]
(0.7, 2.3)	(0.2, 0.6)	(0.4, 2.9)	[87]
0.44	0.04	0.48	[81]
0.13	0.20	0.33	[89]
0.84	4.46	5.30	[90]
$\tau^- \to \eta'\pi^-\nu_\tau$			
$Br_V \times 10^7$	$Br_S \times 10^7$	$Br_{S+V} \times 10^7$	References
< 1	(2, 13)	(2, 14)	[86]
(0.01, 0.34)	(0.6, 1.8)	(0.6, 2.1)	[88]
0.11	0.26	0.37	[81]
2×10^{-5}	4	4	[90]

The obtained results are consistent with the modern experimental constraints [27]

$$Br^{exp}(\tau^- \to \eta\pi^-\nu) < 9.9 \times 10^{-5} , \qquad (116)$$

$$Br^{exp}(\tau^- \to \eta'\pi^-\nu) < 4.0 \times 10^{-6} . \qquad (117)$$

Table 8 provides a comparison with theoretical results of other groups obtained in different phenomenological models. The first two columns in Table 8 show the vector and scalar channel contributions separately. It is seen that in many models the scalar channel dominates over the vector channel for both decay modes. In the ENJL model, a similar situation occurs only in the case of the decay into $\eta'\pi\nu$, while in the case of the η meson, the vector channel contributes most. We note that the problem of describing scalar mesons is currently of great interest due to the uncertainty of the quark composition of these mesons.

5.4 Decay $\tau^- \to \eta(\eta')\pi^-\pi^0\nu_\tau$

In the ENJL model, τ-lepton decays with the creation of a neutrino, η- or η'-mesons, and two pions have a very similar structure to the annihilation processes $e^+e^- \to \eta(\eta')2\pi$ considered in Section 4.5 (see also [72]). As pointed out above, the role of the intermediate photon is here played by a W boson, and instead of neutral ρ mesons, charged mesons participate in these reactions. The corresponding diagrams are similar to those presented in Figs 17 and 18.

The widths of these decays are given by

$$\Gamma(\tau \to \eta(\eta')2\pi\nu) = \frac{3|V_{ud}|^2}{2\pi\alpha^2 m_\tau^8}\, \Gamma(\tau \to e\bar{\nu}_e\nu_\tau) \int_0^{m_\tau} \sigma(q^2)\, dq^2 , \qquad (118)$$

where $\sigma(q^2)$ coincides with cross section (86) for the annihilation process and $\Gamma(\tau \to e\bar{\nu}_e\nu_\tau) = G_F^2 m_\tau^5/(192\pi^3)$. The numerical value obtained for the process with η-meson production is in good agreement with experimental data (Table 9). The prediction obtained in the case with the

Table 9. Partial decay width of $\tau \to \eta(\eta')2\pi\nu$ decays in comparison with experimental data.

Process	NJL model	PDG [27]
$Br(\tau \to \eta 2\pi\nu) \times 10^3$	1.46	1.39 ± 0.10
$Br(\tau \to \eta' 2\pi\nu) \times 10^5$	0.09	< 1.2

η' meson does not contradict experimental upper bounds and can hopefully be checked in the near future.

In [70], these processes are described in the model of resonance chiral Lagrangians with the use of two free parameters, which, however, does not allow the authors to simultaneously describe both decays satisfactorily.

5.5 Decay $\tau^- \to \omega\pi^-\nu_\tau$

The decay $\tau^- \to \omega\pi^-\nu_\tau$ has been studied both experimentally [49, 91] and theoretically (see, e.g., [53, 92–94]). In these papers, phenomenological models with intermediate vector mesons and their radially excited states were used. The structure of the amplitude of this process is similar to that used to describe the process $e^+e^- \to \pi\omega$ in Section 4.3:

$$T = G_F|V_{ud}|\bar{\nu}(1-\gamma^5)\gamma^\mu\tau(T_{W\rho}+T_{\rho'})\epsilon_{\mu\nu\rho\sigma}\,p_\omega^\rho\,p_\pi^\sigma\omega^\nu\pi\,, \quad (119)$$

where p_ω and p_π are momenta of the ω and π mesons. Two contributions to the amplitude, $T_{W\rho}$ and $T_{\rho'}$, are due to the respective intermediate vector mesons $\rho(770)$ and $\rho(1450)$. Here, $T_{W\rho}$ combines contributions from the contact diagram (with an intermediate W boson) and the diagram with an intermediate $\rho(770)$ meson. This leads to a formula with the same structure as that arising in the vector dominance model:

$$T_{W\rho} = \frac{C_\rho}{g_{\rho_1}}\,\frac{1-i\Gamma_\rho/m_\rho}{m_\rho^2-p^2-im_\rho\Gamma_\rho}\,m_\rho^2\,. \quad (120)$$

The factor C_ρ here corresponds to coefficients before the antisymmetric tensor describing the anomalous vertex $\rho\omega\pi$. In the ENJL model,

$$\frac{C_\rho}{g_{\pi_1}} = \left[g_{\rho_1}\frac{\sin(\beta^u+\beta_0^u)}{\sin(2\beta_0^u)}\right]^2 I_3^0 + \left[g_{\rho_2}\frac{\sin(\beta^u-\beta_0^u)}{\sin(2\beta_0^u)}\right]^2 I_3^{(2)} + 2g_{\rho_1}g_{\rho_2}\frac{\sin(\beta^u+\beta_0^u)}{\sin(2\beta_0^u)}\frac{\sin(\beta^u-\beta_0^u)}{\sin(2\beta_0^u)}\,I_3^{(1)}\,. \quad (121)$$

The contribution from the radially excited state $\rho(1450)$ is calculated without using the vector dominance model, by directly calculating the two vertices describing transitions via quark loops $W^- \to \rho'$ and $\rho' \to \omega\pi$ in the ENJL model,

$$T_{\rho'} = C_{\rho'}C_{W\rho'}\,\frac{p^2}{m_{\rho'}^2-p^2-i\sqrt{p^2}\,\Gamma_{\rho'}(p^2)}\,, \quad (122)$$

where $m_{\rho'} = 1465$ MeV and the running width is taken in accordance with a formula in [51]. The factor $C_{\rho'}$ corresponds to the vertex $\rho'\omega\pi$:

$$-\frac{C_{\rho'}}{g_{\pi_1}} = g_{\rho_1}\frac{\sin(\beta^u+\beta_0^u)}{\sin(2\beta_0^u)}\,g_{\rho_1}\frac{\cos(\beta^u+\beta_0^u)}{\sin(2\beta_0^u)}\,I_3^u + g_{\rho_2}\frac{\sin(\beta^u-\beta_0^u)}{\sin(2\beta_0^u)}\,g_{\rho_2}\frac{\cos(\beta^u-\beta_0^u)}{\sin(2\beta_0^u)}\,I_3^u + g_{\rho_1}\frac{\sin(\beta^u+\beta_0^u)}{\sin(2\beta_0^u)}\,g_{\rho_2}\frac{\cos(\beta^u-\beta_0^u)}{\sin(2\beta_0^u)}\,I_3^u + g_{\rho_2}\frac{\cos(\beta^u+\beta_0^u)}{\sin(2\beta_0^u)}\,g_{\rho_1}\frac{\sin(\beta^u-\beta_0^u)}{\sin(2\beta_0^u)}\,I_3^u\,.$$

The factor $C_{W\rho'}$ describes the transition $W \to \rho'$ (see [76] for more details),

$$C_{W\rho'} = -\frac{1}{g_{\rho_1}}\left[\frac{\cos(\beta^u+\beta_0^u)}{\sin(2\beta_0^u)} + R_\rho\,\frac{\cos(\beta^u-\beta_0^u)}{\sin(2\beta_0^u)}\right].$$

Table 10. Partial width and parameters of the process $\tau \to \pi\omega\nu$.

	$g_{\rho\omega\pi}$, GeV^{-1}	Br($\tau \to \pi\omega\nu$), %
NJL	15.40	1.85
CLEO [49]	16.10 ± 0.06	1.95 ± 0.08
Aleph [91]	—	1.91 ± 0.13
SND-2011 [53]	15.75 ± 0.45	—

The width of this process has the form

$$\Gamma(\tau \to \omega\pi\nu) = \frac{1}{4m_\tau}\int\frac{d^3p_\omega}{2E_\omega}\,\frac{d^3p_\pi}{2E_\pi}\,\frac{d^3p_\nu}{2E_\nu} \times \frac{(2\pi)^4\delta^{(4)}(p_\tau-p_\omega-p_\pi-p_\nu)}{(2\pi)^9}\,|T|^2\,.$$

The obtained numerical value for the partial width is presented in Table 10 jointly with experimental results. Apparently, the results of our calculations are in good agreement with experimental data. In addition, in Table 10 we present values of the Wess–Zumino vertex $g_{\rho\omega\pi}$ in comparison with the results obtained by other authors.

5.6 Decay $\tau^- \to f_1\pi^-\nu_\tau$

The τ-lepton decays considered above occurred via intermediate states with vector and scalar mesons in both the ground and first radially excited states. However, there are a number of τ-lepton decays occurring via intermediate states with axial-vector mesons $a_1(1230)$ and $a_1'(1640)$. The mass of the excited state is already close to that of the τ lepton itself. Therefore, it is natural to expect that the contribution to the decay width from such an intermediate state is very insignificant. Hence, we can use the standard NJL model here, ignoring the radially excited states.

Indeed, the widths for decays $\tau \to 3\pi\nu$ [95], $\tau \to \pi\gamma\nu$ [96], and $\tau \to \pi\rho\nu$ [97] calculated in the framework of the standard NJL model are consistent with experimental data. This can be illustrated by the $\tau \to f_1\pi\nu$ decay, which is currently being actively studied (see theoretical [98–100] and experimental [101] papers). We note that a comparison of these calculations in the standard and extended NJL models is given in the electronic preprint of paper [98]. As expected, these results are not significantly different. A similar situation occurs for the calculation of the constant F_π in the $\tau \to \pi\nu$ decay (see Section 5.1).

The amplitude of the considered decay is determined by the Feynman diagrams shown in Figs 27–29 and has the form

$$T_S^\nu = \frac{G_F|V_{ud}|}{g_{\rho_1}}\,L_\mu\big(1+(Q^2-6m_u^2)BW_{a_1}(Q^2) + 6m_u^2BW_{a_1}(Q^2)\big)\,T^{\mu\nu}_{a_1\to f_1\pi}\,,$$
$$T^{\mu\nu}_{a_1\to f_1\pi} = \frac{N_c}{8\pi^2F_\pi}\,\varepsilon_{\mu\nu\alpha\beta}\,p_\alpha q_\beta\,, \quad (123)$$

where p and q are the respective momenta of the pion and the f_1 meson, and $Q = p+q$. What is important here is the description of the transition of the W boson into an a_1 meson in the one-loop quark approximation, which turns out to be proportional to the quantity

$$g_{\mu\nu}Q^2 - Q^\mu Q^\nu + 6m_u^2 g_{\mu\nu}\,.$$

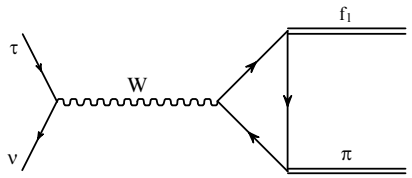

Figure 27. Contact diagram describing the decay $\tau \to f_1\pi\nu_\tau$.

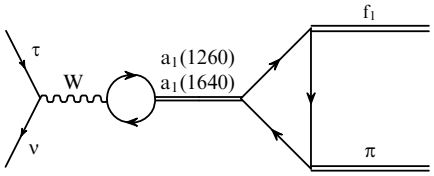

Figure 28. Diagram with an intermediate a_1 meson for the decay $\tau \to f_1\pi\nu_\tau$.

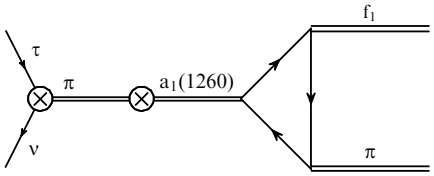

Figure 29. Diagram with the $\pi - a_1$ transition in the intermediate state of the decay $\tau \to f_1\pi\nu_\tau$.

The first two terms represent a gradient-invariant expression, which coincides with the corresponding expression describing transitions of a W boson into a vector ρ meson. The constant term proportional to $6m_u^2$ violates the gradient invariance. However, taking the consecutive transitions of a W boson into a pion and then the pion into an a_1 meson into account (see Fig. 29) gives rise to the appearance of the same constant in the amplitude but with the opposite sign. As a result, the sum of the diagrams shown in Figs 27 and 28 acquires a gradient-invariant form. We note that the product of the part $Q^\mu Q^\nu$ by tensor $T^{\mu\nu}_{a_1\to f_1\pi}$ describing the $a_1 \to f_1\pi$ transition is zero. The remaining sum combined with the contact diagram (see Fig. 27) gives rise to the vector-dominance expression

$$1 + Q^2 \mathrm{BW}_{a_1}(Q^2) = \frac{m_{a_1}^2 - \mathrm{i}m_{a_1}\Gamma_{a_1}}{m_{a_1}^2 - Q^2 - \mathrm{i}m_{a_1}\Gamma_{a_1}}\,.$$

As a result, we obtain the following partial width of this decay: $\mathrm{Br}(\tau \to f_1\pi\nu) = 4.10 \times 10^{-4}$ for the width $\Gamma_{a_1} = 367$ MeV taken from [102]. The experimental value of the partial width of this decay was obtained by the BaBar collaboration from measurements of two decay modes of the f_1 meson [101]:

$$\mathrm{Br}_{\mathrm{exp}}(\tau \to f_1\pi^-\nu_\tau) = \frac{\mathrm{Br}(\tau \to 2\pi^+3\pi^-\nu_\tau)}{\mathrm{Br}(f_1 \to 2\pi^+2\pi^-)}\,,$$

$$\mathrm{Br}_{\mathrm{exp}}(\tau \to f_1\pi^-\nu_\tau) = \frac{\mathrm{Br}(\tau \to \pi^+2\pi^-\eta\nu_\tau)}{\mathrm{Br}(f_1 \to \pi^+\pi^-\eta)}\,.$$

The corresponding values are $(4.73 \pm 0.28 \pm 0.45) \times 10^{-4}$ and $(3.60 \pm 0.18 \pm 0.23) \times 10^{-4}$. Our theoretical result lies between these two experimental values.

This decay was theoretically studied using other approaches in [99, 100]. In [99], an approach similar to the standard NJL model was used, with the resultant partial width 2.91×10^{-4}. In [100], the vector dominance model was used, with the result 1.30×10^{-4}. In both papers, only the contribution from the intermediate $a_1(1260)$ meson without possible $\pi - a_1$ transitions in the intermediate state was taken into account.

5.7 Decays $\tau \to \mathbf{K}^-(\boldsymbol{\pi}^0, \boldsymbol{\eta}, \boldsymbol{\eta}', \mathbf{K}^0)\boldsymbol{\nu}_\tau$

In this section, we discuss τ-lepton decays with the production of two pseudoscalar mesons and a neutrino. In Sections 5.2 and 5.3, we considered such decays without the participation of strange particles. The decays $\tau \to K^-\pi^0\nu_\tau$ [103], $\tau \to K^-(\eta, \eta')\nu_\tau$ [104], and $\tau \to K^-K^0\nu_\tau$ complete the list of such processes.

The characteristic feature of the $\tau \to K^-\pi^0\nu_\tau$ process is a relatively low production threshold of the final products. This implies that the ground states of intermediate mesons lie in the allowed kinematic region and dominate in this decay width in both vector and scalar channels. Therefore, it is sufficient here to use the standard NJL model ignoring the excited states. This assumption is confirmed by a quantitative comparison of the results of calculations in the ENJL model in the appendix of [103].

The vector channel amplitude, including contributions from the contact diagram (Fig. 30) and the diagram with the intermediate K^* meson (Fig. 31), is given by

$$T_V = -\frac{\mathrm{i}}{2} G_F V_{us} \sqrt{Z_\pi Z_K}\, \frac{g(m_u, m_u)}{g(m_u, m_s)} (\bar\nu_\tau \gamma^\mu \tau) \times \left\{ g_{\mu\nu} + \frac{g_{\mu\nu}\left[q^2 - (3/2)(m_s - m_u)^2\right] - q_\mu q_\nu}{M_{K^*}^2 - q^2 - \mathrm{i}\sqrt{q^2}\,\Gamma_{K^*}} \right\} (p_K - p_\pi)^\nu\,, \tag{124}$$

where $V_{us} = 0.2252$ is the Cabbibo–Kobayashi–Maskawa matrix element, $q = p_K + p_\pi$, $M_{K^*} = 892$ MeV, and $\Gamma_{K^*} = 51$ MeV [27]. The first and second terms in the curly brackets correspond to the respective contributions from the intermediate W boson and $K^*(892)$ meson.

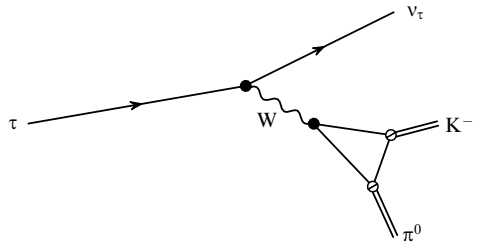

Figure 30. Contact diagram of the $\tau \to K^-\pi^0\nu_\tau$ decay.

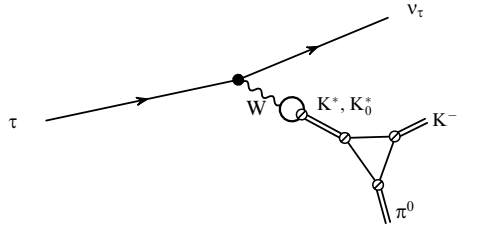

Figure 31. Diagram of the $\tau \to K^-\pi^0\nu_\tau$ decay with intermediate vector (K^*) or scalar (K_0^*) mesons.

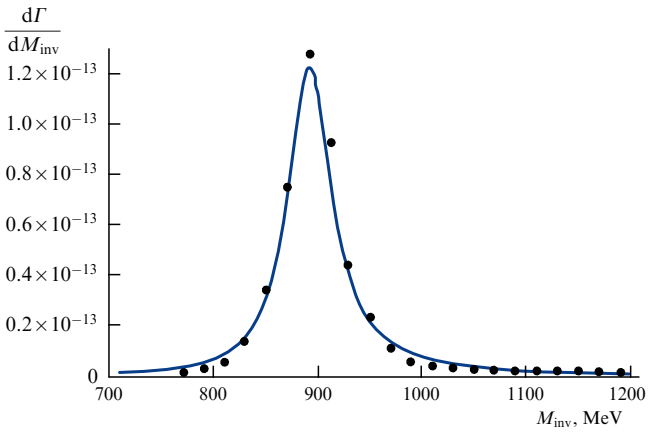

Figure 32. Differential width of the $\tau \to K^-\pi^0\nu_\tau$ decay. M_{inv} is the invariant mass of the pion–kaon system and $d\Gamma/dM_{inv}$ is the dimensionless differential width.

The amplitude of the scalar channel with the intermediate $K_0^*(800)$ meson (see Fig. 31) has the form

$$T_S = -\frac{i}{2} G_F V_{us} \sqrt{Z_\pi Z_K} \frac{g(m_u, m_u)}{g(m_u, m_s)} (\bar\nu_\tau \gamma^\mu \tau) \times \frac{2m_s(m_s - m_u)}{M^2_{K_0^*} - q^2 - i\sqrt{q^2}\,\Gamma_{K_0^*}} q_\mu , \quad (125)$$

where $M_{K_0^*} = 682$ MeV, $\Gamma_{K_0^*} = 547$ MeV [27].

It is interesting to compare individual contributions from the vector and scalar channel to the partial width of the decay considered:

$$\mathrm{Br}(\tau \to K^-\pi^0\nu_\tau)_V = 4.14 \times 10^{-3} , \quad \mathrm{Br}(\tau \to K^-\pi^0\nu_\tau)_S = 0.02 \times 10^{-3} . \quad (126)$$

We see that the vector channel dominates in this case. The full partial width obtained in the standard NJL model,

$$\mathrm{Br}(\tau \to K^-\pi^0\nu_\tau)_{tot} = 4.13 \times 10^{-3} , \quad (127)$$

is in good agreement with the modern experimental value [27]

$$\mathrm{Br}(\tau \to K^-\pi^0\nu_\tau)_{exp} = (4.29 \pm 0.15) \times 10^{-3} . \quad (128)$$

The differential distribution over the invariant mass of the kaon and pion is also found to be consistent with experimental data [106] (Fig. 32).

This decay was considered previously using an NJL-like model [107], where the transition of the W boson into the K^* meson was described by the vector dominance method. As a result, only qualitative agreement with experimental data was reached. As regards the scalar channel, its contribution to the decay width was found to be as small as in our case. In some other papers [108–110], the $\tau \to K\pi\nu_\tau$ decay was described by models like the chiral perturbation theory using additional fitting parameters and form factors.

We next consider the decays $\tau \to K^-\eta\nu_\tau$ and $\tau \to K^-\eta'\nu_\tau$. Recently, the decay $\tau \to K^-\eta\nu_\tau$ has been actively investigated both experimentally [80, 111] and theoretically [104, 112]. A chiral perturbation theory extended by taking resonance states into account was used in [112]. It was argued in [112] that the use of the Breit–Wigner parameterization for the

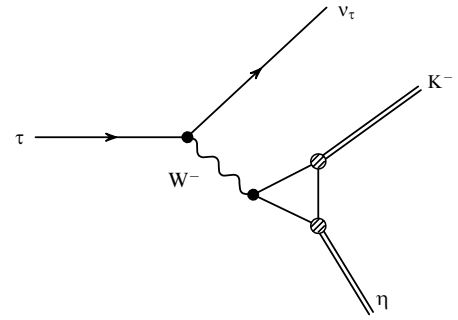

Figure 33. Contact diagram for the process $\tau \to K^-\eta(\eta')\nu_\tau$.

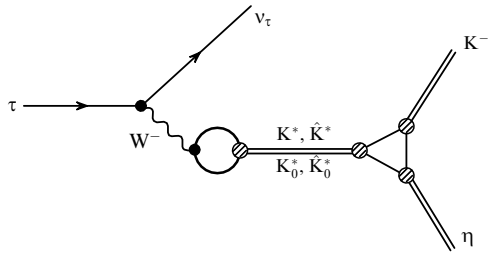

Figure 34. Diagrams for the $\tau \to K^-\eta(\eta')\nu_\tau$ process with an intermediate vector and scalar mesons.

intermediate states of mesons does not allow a satisfactory description of this decay without involving additional form factors. However, it was shown in [104] that the use of the Breit–Wigner parameterization in the ENJL model yields quite reasonable results. Both papers also theoretically predict the $\tau \to K^-\eta'\nu_\tau$ decay width.

The processes $\tau \to K^-\eta\nu_\tau$ and $\tau \to K^-\eta'\nu_\tau$ are described by the Feynman diagrams in Figs 33 and 34. The amplitude corresponding to the sum of contributions from the contact diagram with the intermediate W boson and diagrams with the intermediate vector mesons $K^*(892)$ and $\hat K^* \equiv K^*(1410)$ in the ENJL model has the form

$$T_V = -2iG_F|V_{us}|l^\mu \times \left\{ C_1 g_{\mu\nu} + \frac{C_2 C_3}{g_{K^*}} \frac{g_{\mu\nu}q^2 - q_\mu q_\nu - g_{\mu\nu}(3/2)(m_s - m_u)^2}{M^2_{K^*} - q^2 - i\sqrt{q^2}\,\Gamma_{K^*}} + \frac{C_2' C_3'}{g_{K^*}} \frac{g_{\mu\nu}q^2 - q_\mu q_\nu - g_{\mu\nu}(3/2)(m_s - m_u)^2}{M^2_{\hat K^*} - q^2 - i\sqrt{q^2}\,\Gamma_{\hat K^*}} \right\} (p_K - p_\eta)^\nu , \quad (129)$$

where $l^\mu = \bar\nu_\tau \gamma^\mu \tau$ is the lepton current, $q = p_K + p_\eta$, $M_{K^*} = 896$ MeV, $M_{\hat K^*} = 1414$ MeV, $\Gamma_{K^*} = 46$ MeV, and $\Gamma_{\hat K^*} = 232$ MeV are the masses and widths of the vector mesons [27]. The scalar channel amplitude includes contributions from the intermediate $K_0^*(800)$ and $K_0^*(1430)$mesons:

$$T_S = -4iG_F|V_{us}|l^\mu \left\{ \frac{C_4 C_5}{g_{K_0^*}} \frac{m_s - m_u}{M^2_{K_0^*} - q^2 - i\sqrt{q^2}\,\Gamma_{K_0^*}} + \frac{C_4' C_5'}{g_{K_0^*}} \frac{m_s - m_u}{M^2_{\hat K_0^*} - q^2 - i\sqrt{q^2}\,\Gamma_{\hat K_0^*}} \right\} q_\mu .$$

Explicit formulas for the coefficients $C_{2,3,4,5}$ and $C'_{2,3,4,5}$ can be found in [104].

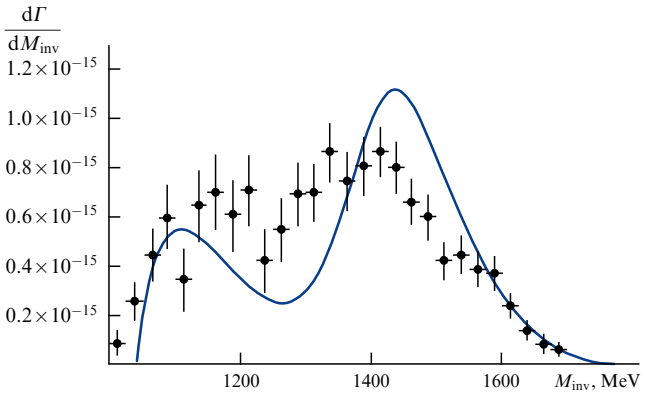

Figure 35. Differential width of the $\tau \to \eta K^- \nu_\tau$ decay.

We obtain the following estimates for the corresponding contributions to the partial width of the decay $\tau \to \eta K^- \nu_\tau$:

$$\mathrm{Br}(\tau \to \eta K^- \nu_\tau)_V = 1.46 \times 10^{-4}\,,$$
$$\mathrm{Br}(\tau \to \eta K^- \nu_\tau)_S = 0.28 \times 10^{-7}\,.$$

The total value with account for interference,

$$\mathrm{Br}(\tau \to \eta K^- \nu_\tau)_{\mathrm{tot}} = 1.45 \times 10^{-4}\,, \qquad (130)$$

is in good agreement with experimental data:

$$\mathrm{Br}(\tau \to \eta K^- \nu_\tau)_{\mathrm{exp}} = (1.58 \pm 0.14) \times 10^{-4}\ \ [111]\,,$$
$$\mathrm{Br}(\tau \to \eta K^- \nu_\tau)_{\mathrm{exp}} = (1.42 \pm 0.18) \times 10^{-4}\ \ [80]\,,$$
$$\mathrm{Br}(\tau \to \eta K^- \nu_\tau)_{\mathrm{exp}} = (1.52 \pm 0.08) \times 10^{-4}\ \ [27]\,.$$

Figure 35 shows a comparison of theoretical predictions (solid curve) for the differential distribution of the considered decay with respect to the invariant mass of the final meson pair with experimental data [111] (black dots with error bars). The visible deviation of the theoretical curve from experimental points is likely to be due to the nonoptimal choice of the width and mass of the excited K_0^* meson.

In a similar way, the partial width of the $\tau \to \eta' K^- \nu_\tau$ decay is theoretically predicted to be

$$\mathrm{Br}(\tau \to \eta' K^- \nu_\tau) = 1.25 \times 10^{-6}\,. \qquad (131)$$

Presently, there are only experimental upper bounds on this quantity [27]:

$$\mathrm{Br}(\tau \to \eta' K^- \nu_\tau)_{\mathrm{exp}} < 2.4 \times 10^{-6}\,. \qquad (132)$$

This gives hope to check the theoretical prediction very soon. We note that a similar value was calculated in [112]: $\mathrm{Br}(\tau \to \eta' K^- \nu_\tau) = 1.03(+0.37/-0.29) \times 10^{-6}$.

To conclude the description of τ-lepton decays into two pseudoscalar mesons and a neutrino, we consider the decay $\tau \to K^0 K^- \nu_\tau$. The process $\tau \to K^0 K^- \nu_\tau$ differs from above reactions by being dominated by the vector channel contributions containing nonstrange vector mesons $\rho^-(770)$ and $\rho^-(1450)$. The scalar channel contribution to this decay can be totally ignored because the transition probability of a W boson into a scalar meson is here proportional to the small mass difference of the light d and u quarks. Figure 36 shows a contact diagram with the transition of the W boson into a pair

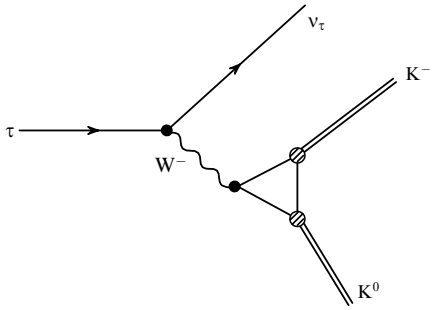

Figure 36. Feynman diagram for the $\tau \to K^0 K^- \nu_\tau$ contact decay.

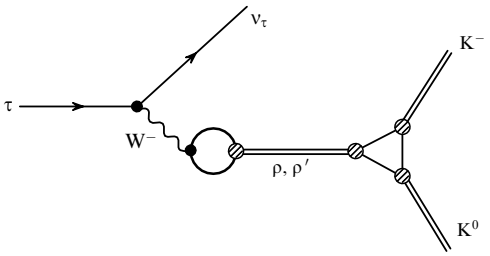

Figure 37. Feynman diagram for the decay $\tau \to K^0 K^- \nu_\tau$ with intermediate $\rho(770)$ and $\rho(1450)$ mesons.

of kaons via the triangle quark loop. Figure 37 presents the diagram with intermediate vector mesons. The amplitude of the process is expressed as

$$T = -2\sqrt{2}\,\mathrm{i} G_F |V_{ud}| l^\mu \times \left\{ I_{KK W} g_{\mu\nu} + \frac{I_{KK\rho} C_\rho}{g_\rho} \frac{g_{\mu\nu} q^2 - q_\mu q_\nu}{M_\rho^2 - q^2 - \mathrm{i}\sqrt{q^2}\,\Gamma_\rho} + \frac{I_{KK\rho'} C_{\rho'}}{g_\rho} \frac{g_{\mu\nu} q^2 - q_\mu q_\nu}{M_{\rho'}^2 - q^2 - \mathrm{i}\sqrt{q^2}\,\Gamma_{\rho'}} \right\} (p_{K^0} - p_{K^-})^\nu\,,$$

where

$$C_\rho = \frac{1}{\sin(2\beta_0^u)} \left[\sin(\beta^u + \beta_0^u) + R_{V_u} \sin(\beta^u - \beta_0^u) \right], \qquad (133)$$
$$C_{\rho'} = -\frac{1}{\sin(2\beta_0^u)} \left[\cos(\beta^u + \beta_0^u) + R_{V_u} \cos(\beta^u - \beta_0^u) \right]$$

describe the $W-\rho$ transitions, and the diverging part of the integral over the triangle quark loop has the form

$$I_{KKV}\Big|_{V=\rho,\rho',W} = -\mathrm{i}\,\frac{N_c}{(2\pi)^4} \times \int \mathrm{d}^4 k\, \frac{a_K^2(\mathbf{k}^2) b_V(\mathbf{k}^2)}{(m_s^2 - k^2)(m_u^2 - k^2)}\, \Theta(\Lambda_3^2 - \mathbf{k}^2)\,,$$

$$a_K(\mathbf{k}^2) = \frac{1}{\sin(2\theta_K^0)} \left[g_K \sin(\theta_K + \theta_K^0) + g_K' f_a(\mathbf{k}^2) \sin(\theta_K - \theta_K^0) \right],$$

$$b_\rho(\mathbf{k}^2) = \frac{1}{\sin(2\beta_0^u)} \left[g_{\rho_1} \sin(\beta^u + \beta_0^u) + g_{\rho_2} f_a(\mathbf{k}^2) \sin(\beta^u - \beta_0^u) \right],$$

Table 11. Partial $\tau \to K^0K^-\nu_\tau$ decay width.

	Br ($\times 10^{-4}$)	References
Theory	27	[99]
	12.5 ± 1.3	[114]
	13.5/19	[115]
	16	[116]
	12.7 ± 2.5	[102]
Experiment	15.1 ± 4.3	[113]
	16.2 ± 3.2	[117]
	14.8 ± 0.68	[118]
	14.9 ± 0.5	[27]

$$b_{\rho'}(\mathbf{k}^2) = -\frac{1}{\sin(2\beta_0^{\rm u})}\left[g_{\rho_1}\cos(\beta^{\rm u}+\beta_0^{\rm u}) + g_{\rho_2} f_{\rm a}(\mathbf{k}^2)\cos(\beta^{\rm u}-\beta_0^{\rm u})\right],$$

$$b_{\rm W}(\mathbf{k}^2) = 1\,. \qquad (134)$$

As a result, for the decay $\tau \to K^0K^-\nu_\tau$, we obtain [105]

$$\mathrm{Br}(\tau \to K^0K^-\nu_\tau) = (12.7 \pm 2.5) \times 10^{-4}\,. \qquad (135)$$

A comparison of the partial width of this decay calculated in different models with experimental data is presented in Table 11. We note that the experimental mass and especially width of the excited $\rho(1450)$ meson have large errors. This leads to a high uncertainty in the theoretical partial width (135), which we have estimated by varying parameters $M_{\rho'}$ and $\Gamma_{\rho'}$ within the error limits.

The differential distribution of the considered decay width with respect to the invariant mass of the kaon pair is shown in Fig. 38 in comparison with experimental data [113]. The solid curve corresponds to theoretical predictions obtained for the central values of the mass and width of the $\rho(1450)$ meson, and the dashed curve is calculated for the particular example $M_{\rho'} = 1440$ MeV and $\Gamma_{\rho'} = 340$ MeV.

To conclude this section, we note that because the τ lepton has a very large number of decay modes, we restricted ourselves to considering only a few examples of such processes in order to demonstrate the possibility of their description by different phenomenological models. We have shown that the ENJL model permits a quite satisfactory description of all these decays using a minimal set of model parameters that remain fixed when considering different processes. This provides a greater predictability with this model than with other phenomenological approaches.

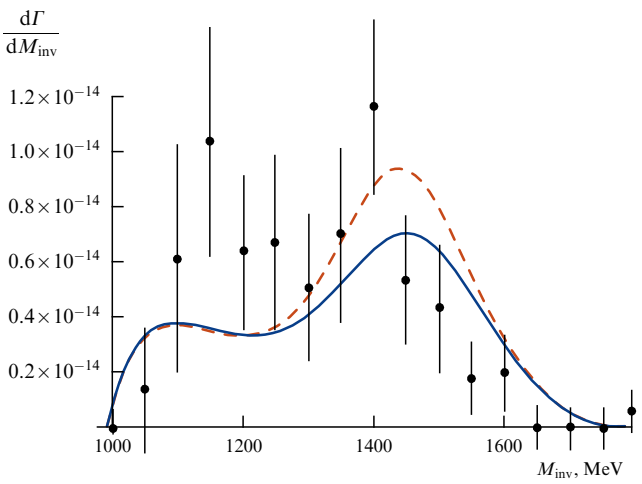

Figure 38. Differential width of the $\tau \to K^0K^-\nu_\tau$ decay vs the invariant mass of K^0K^-.

6. Conclusion

As noted in the Introduction, to describe the low-energy physics of mesons, various phenomenological models are used, which are typically based on the chiral symmetry of strong interactions and on the vector dominance model. The Nambu–Jona-Lasinio model based on chiral symmetry breaking is one of the most successful phenomenological models. It has the minimal number of arbitrary parameters and hence a greater predictability.

Recently, many theoretical and experimental studies have been focused on the production of mesons in electron–positron annihilations at low energies, as well as in τ-lepton decays. In these processes, intermediate mesons, both in the ground and first radially excited states, play the crucial role. To describe the radially excited states of mesons, many authors use additional free parameters. At the same time, in papers by Volkov and Weiss [17, 18] published in 1997, an extended NJL model was proposed that describes both the ground and first radially excited states of mesons in the framework of the chiral-symmetric approach. The number of additional parameters increases insignificantly. The additional parameters were used here only to describe the mass spectrum of excited mesons. This enabled us to describe the main decay modes of the radially excited mesons, as well as their interactions with other mesons. In addition, the extended NJL models proved to be very effective in describing e^-e^+ annihilations and τ-lepton decays, which is demonstrated in this review.

The NJL model can describe meson properties not only in the vacuum but also in a hot dense medium [11, 20, 119, 120]. Presently, this field of physics is being intensively studied. In particular, the threshold of the phase transition of the hadronic matter into the quark–gluon plasma is being determined. Here, the NJL model is also successfully applied.

The authors thank E A Kuraev, D G Kostyunin, and A A Pivovarov for the fruitful collaboration.

References

1. Gell-Mann M, Oakes R J, Renner B *Phys. Rev.* **175** 2195 (1968)
2. Sakurai J J *Ann. Physics* **11** 1 (1960)
3. Nambu Y, Jona-Lasinio G *Phys. Rev.* **122** 345 (1961)
4. Eguchi T *Phys. Rev. D* **14** 2755 (1976)
5. Kikkawa K *Prog. Theor. Phys.* **56** 947 (1976)
6. Ebert D, Volkov M K *Z. Phys. C* **16** 205 (1983)
7. Volkov M K *Ann. Physics* **157** 282 (1984)
8. Volkov M K *Sov. J. Part. Nucl.* **17** 186 (1986); *Fiz. Elem. Chastits At. Yadra* **17** 433 (1986)
9. Ebert D, Reinhardt H *Nucl. Phys. B* **271** 188 (1986)
10. Klevansky S P *Rev. Mod. Phys.* **64** 649 (1992)
11. Volkov M K, Radzhabov A E *Phys. Usp.* **49** 551 (2006); *Usp. Fiz. Nauk* **176** 569 (2006)
12. Volkov M K *Phys. Part. Nucl.* **24** 35 (1993); *Fiz. Elem. Chastirs At. Yadra* **24** 81 (1993)
13. Arbuzov B A, Volkov M K, Zaitsev I V *Int. J. Mod. Phys. A* **21** 5721 (2006)
14. Volkov M K, Ebert D *Sov. J. Nucl. Phys.* **36** 736 (1982); *Yad. Fiz.* **36** 1265 (1982)
15. Ebert D, Reinhardt H, Volkov M K *Prog. Part. Nucl. Phys.* **33** 1 (1994)
16. Volkov M K, Yudichev V L *Phys. Part. Nucl.* **31** 282 (2000); *Fiz. Elem. Chastits At. Yadra* **31** 576 (2000); hep-ph/9906371

17. Volkov M K, Weiss C *Phys. Rev. D* **56** 221 (1997); hep-ph/9608347
18. Volkov M K *Phys. Atom. Nucl.* **60** 1920 (1997); *Yad. Fiz.* **60** 2094 (1997)
19. Volkov M K, Ebert D, Nagy M *Int. J. Mod. Phys. A* **13** 5443 (1998)
20. Ebert D, Kalinovsky Y L, Münchow L, Volkov M K *Int. J. Mod. Phys. A* **8** 1295 (1993)
21. 't Hooft G *Phys. Rev. Lett.* **37** 8 (1976)
22. Vogl U, Weise W *Prog. Part. Nucl. Phys.* **27** 195 (1991)
23. Sakurai J J *Currents and Mesons* (Chicago Lectures in Physics) (Chicago: Univ. of Chicago Press, 1969)
24. Volkov M K, Yudichev V L *Phys. Atom. Nucl.* **62** 1567 (1999); *Yad. Fiz.* **62** 1674 (1999)
25. Volkov M K, Yudichev V L *Phys. Atom. Nucl.* **63** 1835 (2000); *Yad. Fiz.* **63** 1924 (2000)
26. Volkov M K, Yudichev V L *Eur. Phys. J. A* **10** 109 (2001)
27. Olive K A et al. (Particle Data Group) *Chin. Phys. C* **38** 090001 (2014)
28. Treiman S B, Jackiw R, Gross D J *Lectures on Current Algebra and Its Applications* (Princeton, NJ: Princeton Univ. Press, 1972)
29. Kuraev E A, Volkov M K *Phys. Lett. B* **682** 212 (2009)
30. Arbuzov A B, Volkov M K *Phys. Rev. C* **84** 058201 (2011)
31. Vishneva A V, Volkov M K *Phys. Part. Nucl. Lett.* **11** 352 (2014); *Pis'ma Fiz. Elem. Chastits At. Yadra* **11** 560 (2014)
32. Brodsky S J, Kinoshita T, Terazawa H *Phys. Rev. Lett.* **25** 972 (1970)
33. Roe N A et al. *Phys. Rev. D* **41** 17 (1990)
34. Gronau M, Rosner J L *Phys. Rev. D* **79** 074006 (2009)
35. Achasov N N, Kozhevnikov A A *Int. J. Mod. Phys. A* **7** 4825 (1992)
36. Achasov M N et al. *Eur. Phys. J. C* **12** 25 (2000)
37. Achasov M N et al. *Phys. Lett. B* **559** 171 (2003)
38. Akhmetshin R R et al. (CMD-2 Collab.) *Phys. Lett. B* **509** 217 (2001)
39. Achasov M N et al. *Phys. Rev. D* **74** 014016 (2006)
40. Ahmadov A I, Kostunin D G, Volkov M K *Phys. Rev. C* **87** 045203 (2013); *Phys. Rev. C* **89** 039901 (2014) Erratum
41. Bisello D (DM2 Collab.) *Nucl. Phys. B Proc. Suppl.* **21** 111 (1991)
42. Dolinsky S I et al. *Phys. Rep.* **202** 99 (1991)
43. Achasov M N et al. *Phys. Lett. B* **486** 29 (2000)
44. Akhmetshin R R et al. (CMD-2 Collab.) *Phys. Lett. B* **562** 173 (2003)
45. Gerasimov S B, Govorkov A B *Z. Phys. C* **13** 43 (1982)
46. Close F E, Donnachie A, Kalashnikova Yu S *Phys. Rev. D* **65** 092003 (2002)
47. Li G, Zhang Y J, Zhao Q *J. Phys. G* **36** 085008 (2009)
48. Ambrosino F et al. (KLOE Collab.) *Phys. Lett. B* **669** 223 (2008)
49. Edwards K W et al. (CLEO Collab.) *Phys. Rev. D* **61** 072003 (2000)
50. Kittimanapun K et al. *Phys. Rev. C* **79** 025201 (2009)
51. Arbuzov A B, Kuraev E A, Volkov M K *Phys. Rev. C* **83** 048201 (2011)
52. Volkov M K, Arbuzov A B, Kostunin D G *Phys. Rev. D* **86** 057301 (2012)
53. Achasov M N et al. *Chin. Phys. C* **36** 573 (2012)
54. Ahmadov A I, Kuraev E A, Volkov M K *Phys. Part. Nucl. Lett.* **9** 461 (2012); *Pis'ma Fiz. Elem. Chastis At. Yadra* **9** 756 (2012)
55. Achasov M N et al. *JETP* **101** 1053 (2005); *Zh. Eksp. Teor. Fiz.* **128** 1201 (2005)
56. Gounaris G J, Sakurai J J *Phys. Rev. Lett.* **21** 244 (1968)
57. Kuhn J H, Santamaria A *Z. Phys. C* **48** 445 (1990)
58. O'Connell H B et al. *Prog. Part. Nucl. Phys.* **39** 201 (1997)
59. Dominguez C A et al. *Phys. Rev. D* **76** 095002 (2007)
60. Jegerlehner F, Szafron R *Eur. Phys. J. C* **71** 1632 (2011)
61. Achasov N N, Kozhevnikov A A *Phys. Rev. D* **83** 113005 (2011); *Phys. Rev. D* **85** 019901 (2012)
62. Volkov M K, Kostunin D G *Phys. Rev. C* **86** 025202 (2012)
63. Arbuzov A B, Kuraev E A, Volkov M K *Eur. Phys. J. A* **47** 103 (2011)
64. Ebert D, Ivanov A N, Reinhardt H, Volkov M K *Phys. Lett. B* **182** 193 (1986)
65. Cordier A et al. (DM1 Collab.) *Nucl. Phys. B* **172** 13 (1980)
66. Antonelli A et al. (DM2 Collab.) *Phys. Lett. B* **212** 133 (1988)
67. Druzhinin V P et al. (ND Collab.) *Phys. Lett. B* **174** 115 (1986)
68. Akhmetshin R R et al. (CMD-2 Collab.) *Phys. Lett. B* **489** 125 (2000)
69. Aubert B et al. (BaBar Collab.) *Phys. Rev. D* **76** 092005 (2007)
70. Dumm D G, Roig P *Phys. Rev. D* **86** 076009 (2012)
71. Dai L Y, Portolés J, Shekhovtsova O *Phys. Rev. D* **88** 056001 (2013)
72. Volkov M K, Arbuzov A B, Kostunin D G *Phys. Rev. C* **89** 015202 (2014)
73. Ahmadov A I, Volkov M K *Phys. Part. Nucl. Lett.* **12** 744 (2015); *Pis'ma Fiz. Elem. Chastis At. Yadra* **12** 1153 (2015)
74. Asner D M et al. (CLEO Collab.) *Phys. Rev. D* **61** 012002 (2000)
75. Ahmadov A I, Kalinovsky Y L, Volkov M K *Int. J. Mod. Phys. A* **30** 1550161 (2015)
76. Volkov M K, Kostunin D G *Phys. Part. Nucl. Lett.* **10** 7 (2013); *Pis'ma Fiz. Elem. Chastits At. Yadra* **10** 18 (2013)
77. Anderson S et al. (CLEO Collab.) *Phys. Rev. D* **61** 112002 (2000)
78. Schael S et al. (ALEPH Collab.) *Phys. Rep.* **421** 191 (2005)
79. Fujikawa M et al. (The Belle Collab.) *Phys. Rev. D* **78** 072006 (2008)
80. del Amo Sanchez P et al. (BaBar Collab.) *Phys. Rev. D* **83** 032002 (2011)
81. Volkov M K, Kostunin D G *Phys. Rev. D* **86** 013005 (2012)
82. Tisserant S, Truong T N *Phys. Lett. B* **115** 264 (1982)
83. Bramon A, Narison S, Pich A *Phys. Lett. B* **196** 543 (1987)
84. Neufeld H, Rupertsberger H *Z. Phys. C* **68** 91 (1995)
85. Nussinov S, Soffer A *Phys. Rev. D* **78** 033006 (2008)
86. Nussinov S, Soffer A *Phys. Rev. D* **80** 033010 (2009)
87. Paver N, Riazuddin *Phys. Rev. D* **82** 057301 (2010)
88. Paver N, Riazuddin *Phys. Rev. D* **84** 017302 (2011)
89. Descotes-Genon S, Moussallam B *Eur. Phys. J. C* **74** 2946 (2014)
90. Escribano R, Gonzàlez-Solís S, Roig P *Phys. Rev. D* **94** 034008 (2016); arXiv:1601.03989
91. Buskulic D et al. (ALEPH Collab.) *Z. Phys. C* **74** 263 (1997)
92. López Castro G, López Falcón D A *Phys. Rev. D* **54** 4400 (1996)
93. Flores-Tlalpa A, López-Castro G *Phys. Rev. D* **77** 113011 (2008)
94. Guo Z-H *Phys. Rev. D* **78** 033004 (2008)
95. Ivanov Yu P, Osipov A A, Volkov M K *Z. Phys. C* **49** 563 (1991)
96. Ivanov Yu P, Osipov A A, Volkov M K *Phys. Lett. B* **242** 498 (1990)
97. Volkov M K, Ivanov Yu P, Osipov A A, Preprint P2-89-419 (Dubna: JINR, 1989)
98. Kostunin D G, Vishneva A V, Volkov M K *Eur. Phys. J. A* **50** 137 (2014)
99. Li B A *Phys. Rev. D* **55** 1436 (1997)
100. Calderón G, Muñoz J H, Vera C E *Phys. Rev. D* **87** 114011 (2013)
101. Lees J P et al. (BaBar Collab.) *Phys. Rev. D* **86** 092010 (2012)
102. Alekseev M G et al. (COMPASS Collab.) *Phys. Rev. Lett.* **104** 241803 (2010)
103. Volkov M K, Pivovarov A A *Mod. Phys. Lett. A* **31** 1650043 (2016)
104. Volkov M K, Pivovarov A A *JETP Lett.* **103** 613 (2016); *Pis'ma Zh. Eksp. Teor. Fiz.* **103** 697 (2016)
105. Volkov M K, Pivovarov A A *Mod. Phys. Lett. A* **31** 1650138 (2016)
106. Aubert B et al. (BaBar Collab.) *Phys. Rev. D* **76** 051104(R) (2007)
107. Bednyakov V A, Osipov A A, JINR Communication E2-92-16 (Dubna: JINR, 1992)
108. Finkemeier M, Mirkes E *Z. Phys. C* **72** 619 (1996)
109. Jamin M, Pich A, Portoles J *Phys. Lett. B* **664** 78 (2008)
110. Boito D R, Escribano R, Jamin M *JHEP* **2010** (09) 031 (2010)
111. Inami K et al. (Belle Collab.) *Phys. Lett. B* **672** 209 (2009)
112. Escribano R, González-Solís S, Roig P *JHEP* **2013** (10) 039 (2013)
113. Coan T E et al. (CLEO Collab.) *Phys. Rev. D* **53** 6037 (1996)
114. Palomar J E *Nucl. Phys. B Proc. Suppl.* **121** 183 (2003); hep-ph/0202203
115. Czyż H, Grzelińska A, Kühn J H *Phys. Rev. D* **81** 094014 (2010)
116. Dubnička S, Dubničková A Z *Acta Phys. Slov.* **60** 1 (2010)
117. Barate R et al. (ALEPH Collab.) *Eur. Phys. J. C* **10** 29 (1999)
118. Ryu S et al. (Belle Collab.) *Phys. Rev. D* **89** 072009 (2014)
119. Hatsuda T, Kunihiro T *Phys. Rep.* **247** 221 (1994)
120. Kalinovsky Yu L, Toneev V D, Friesen A V *Phys. Usp.* **59** 367 (2016); *Usp. Fiz. Nauk* **186** 387 (2016)